Computational Study of the Oxygen Initiated Decomposition of 2-Oxepinoxy Radical: A Key Intermediate in the Oxidation of Benzene

John K. Merle and Christopher M. Hadad*

Department of Chemistry, 100 West 18th Avenue, The Ohio State University, Columbus, Ohio 43210

Received: June 20, 2004; In Final Form: July 23, 2004

Density functional theory was utilized to determine whether the addition of $O_2(^3\Sigma_g)$ to 2-oxepinoxy radical, a proposed intermediate in the unimolecular decomposition of phenylperoxy radical, followed by unimolecular rearrangement and decomposition results in the formation of experimentally detected C_1-C_5 products via oxidative combustion of benzene. B3LYP/6-31G* geometries for possible pathways resulting from the initial formation of 1,2-dioxetanyl, 1,3-peroxy, 1,4-peroxy, hydroperoxy, and peroxy moiety scission intermediates were calculated. Energies were determined by B3LYP/6-311+G** single-point energy calculations on the B3LYP/6-31G* geometries. For the O_2 addition steps and most favored pathway, the B3LYP/6-31G* geometries were reoptimized and energies obtained via the CBS-QB3 method. The B3LYP/6-31G* geometries were also used to obtain the energetic parameters to generate the free energy profiles for all pathways at 298, 500, 750, 1000, and 1250 K. For temperatures between 298 and 750 K, the formation of peroxyoxepinone radicals and their decomposition pathways and products are competitive with those proposed by Fadden for the unimolecular decomposition of 2-oxepinoxy radical. However, a large entropic penalty, associated with the step for O_2 addition to 2-oxepinoxy radical, is incurred at higher temperatures, thereby making these pathways less competitive as the temperature rises. At temperatures <1250 K, the same pathway maintains the lowest overall free energy profile and corresponds to rearrangement of 6-peroxyoxepinone (**1c**) to form a 1,4-peroxy intermediate between the ring carbons adjacent to the ester moiety (**15a**), followed by release of CO_2 to form 5-oxapentenal radical (**21c**), which then cyclizes (**22c**) and releases formyl radical, thereby generating furan, CO_2, and formyl radical as final products (**10a**). At 1250 K, all pathways proceeding from 2-peroxyoxepinone (**1a**) and through the peroxy bond scission intermediate (**16a**) have the lowest free energy profile.

I. Introduction

For years, chemists have been working toward an understanding of the oxidation of aromatic compounds. Aromatic compounds are major constituents in various fuels, including coal and gasoline, thereby consumed by combustion processes to generate energy for numerous uses.[1,2] Benzene, as well as toluene and other mono- and dialkyl benzenes, have been shown to be present in air masses around industrial regions in significant amounts.[1,3] Most of their presence can be attributed to incomplete decomposition of the fuel during combustion.[3,4] Benzene and benzene derivatives have also been shown to aggregate into polycyclic aromatic hydrocarbons (PAHs) in pyrolysis environments. Heavy PAHs, in turn, can act as seeds for the formation of particles of soot, which leads to poor local and regional air quality and has adverse effects on human health.[5,6] An understanding of the processes involved during the combustion and oxidation of aromatic compounds is necessary to control their emission and influence on air quality.

Due to the prominence of aromatics in fuels, the oxidation of benzene, the most basic aromatic compound, has been the subject of numerous studies. Experimental studies using mass spectrometric detection[7−11] at high to intermediate temperatures and various fuel/oxidant ratios indicate that the most common products of benzene oxidation are CO_2, CO, C_2H_2 (acetylene), cyclopentadienyl radical, and various unsaturated C_2O_x and C_3O_x species. The commonly accepted high-temperature mechanism for the initiation reaction of benzene oxidation with molecular oxygen results in the generation of phenyl and hydroperoxyl radicals (eq 1)[7,10] followed by the addition of molecular oxygen and concomitant or simultaneous loss of oxygen atom (^3P) (eq 2).[7−9]

$$C_6H_6 + O_2 \rightarrow C_6H_5 + HO_2 \quad (1)$$

$$C_6H_5 + O_2 \rightarrow C_6H_5O + O(^3P) \quad (2)$$

Yu and Lin,[12] however, successfully performed kinetic studies to determine the rate of reaction of phenyl radical with O_2 using cavity ring-down (CRD) spectroscopy and detected phenylperoxy radical at temperatures as high as 473 K. Using a flow system to analyze the reaction of benzene and O_2 in a nitrogen diluent at 685 K, Norrish and Taylor[13] predicted that phenylperoxy radical was a probable intermediate by identification of *o*- and *p*-dihydroxybenzenes formed as products.

Computational methods have also been utilized to determine the most thermodynamically and kinetically viable mechanistic pathways involved in benzene oxidation.[14−20] Theoretical studies by this group,[15] based on B3LYP/6-311+G**//B3LYP/6-31G* free energies, predicted that the phenylperoxy radical is the more thermodynamically favored intermediate, relative to phenoxy radical, at $T \leq \sim 450$ K, whereas at $T > 450$ K, entropy dominates, thereby making phenoxy radical the preferred intermediate based on free energies. However, kinetic barriers were significant. This implies that under low-temperature

* Corresponding author. E-mail: hadad.1@osu.edu. Fax: (614) 292-1685.

10.1021/jp047317w CCC: $27.50
Published on Web 09/10/2004

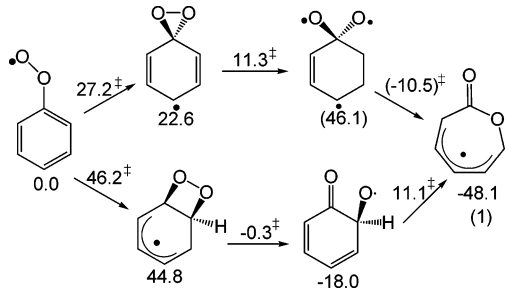

Figure 1. Reaction scheme for the generation of 2-oxepinoxy radical (**1**). Energies are at the B3LYP/6-311+G**//B3LYP/6-31G* level ΔG(298 K) relative to phenylperoxy radical.

combustion and atmospheric conditions, phenylperoxy radical is likely to play an important role in the decomposition of phenyl radical.

Carpenter[14] utilized PM3/UHF semiempirical calculations to elucidate possible decomposition pathways for phenylperoxy radical to form cyclopentadienyl radical and CO_2. He considered a pathway in which phenylperoxy radical rearranges to form a spirodioxiranyl radical intermediate, with an enthalpic barrier of 26.1 kcal/mol, to form a thermodynamically stable seven-membered ring radical, 2-oxepinoxy (**1**), as shown in Figure 1. Barckholtz et al. and Fadden et al. have refined the Carpenter pathway energies using density functional theory and high-level ab initio calculations to study this decomposition process as well as to probe for the formation of a dioxetanyl radical intermediate leading to 2-oxepinoxy radical (**1**).[15,16] Decomposition through a spirodioxiranyl radical was shown to be the most viable reaction path leading to 2-oxepinoxy radical, with a free energy barrier of ~41.6 kcal/mol at 298 K, due to the inclusion of an additional high-energy tri-radical intermediate (Figure 1).[16] Despite the inclusion of the high-energy tri-radical species, the spirodioxiranyl pathway exhibited a lower barrier than that for the formation of phenoxy radical and oxygen atom, which has a calculated free energy barrier of ~51.0 kcal/mol.[16] These barriers are rough estimates, however, because of spin contamination in the wave functions of these key intermediates. At the B3LYP/6-311+G**//B3LYP/6-31G* level, 2-oxepinoxy radical was calculated to have a ΔG(298 K) energy of −79.9 kcal/mol with respect to infinitely separated phenyl radical and $O_2(^3\Sigma_g)$ reactants.[16] Consistent values were obtained with UMP4(SDQ)/6-31G** and UCCSD(T)/6-31G** energy calculations in the same study. Mebel and Lin[18] in a theoretical study of $C_6H_5O_2$ geometrical isomers estimated 2-oxepinoxy radical (**1**) to have a ΔH(0 K) of −91.8 kcal/mol, with respect to phenyl radical and molecular oxygen, based on PUMP3/6-31G*//UHF/6-31G* energies. The stability of 2-oxepinoxy radical indicates that it should be relatively long-lived after its initial formation and therefore potentially susceptible to further oxidation by reactive species with appreciable concentration contained in a typical radical pool.

In this study, we utilized the B3LYP hybrid density functional theory method to analyze the potential energy surface for the decomposition of 2-oxepinoxy radical after further addition of O_2 ($^3\Sigma_g$). The energies of stationary points for these decomposition pathways following the initial formation of 1,2-dioxetanyl, 1,3-peroxy, and 1,4-peroxy intermediates, as well as scission of the O−O peroxy bond and abstraction of an H-atom by the geminal peroxy moiety, were examined. The energies for these surfaces were evaluated at $T = 298-1250$ K, the range in which phenylperoxy radical has been shown to be a viable combustion component to determine the viability of these pathways.

II. Computational Details

All geometry optimizations and energy and frequency calculations were performed using Gaussian98[21] at the Ohio Supercomputer Center or on IBM RS/6000 workstations. Stationary points were determined using B3LYP hybrid density functional theory (DFT) with the 6-31G* basis set.[22−24] The B3LYP functional has been shown to evaluate aromatic C−H and other homolytic bond dissociation energies accurately relative to more expensive high-level ab initio methods with minimal cost and spin contamination.[17,20,25] In general, $\langle S^2 \rangle$ values were as expected and typically were $0.75 \leq \langle S^2 \rangle \leq 0.80$, except were noted in the text. Frequency calculations were performed on all stationary points to confirm the nature of the geometry. Minima were confirmed to have all real vibrational frequencies. All transition state geometries were confirmed to have a single imaginary vibrational frequency corresponding to motion along the reaction coordinate and were further shown to connect the proper reactant and product by displacement along the transition vector for the imaginary frequency in both the positive and negative directions (typically 10%), followed by careful optimization using either of the calcfc or calcall options. Alternatively, intrinsic reaction coordinate (IRC)[26] calculations were performed for the more difficult cases. Single-point energy calculations on each stationary point were calculated at the B3LYP/6-311+G** level with the scf = tight option. All basis sets for these B3LYP calculations used six Cartesian d functions.

The Thermo94[27] program was used to determine the thermal contributions to the Gibbs free energy in the temperature range from 298 to 1250 K. (The Supporting Information provides all of the enthalpic and free energy corrections at different temperatures.) All thermal contributions were calculated using unscaled[28] harmonic vibrational frequencies and rotational constants derived from the B3LYP/6-31G* geometries and assuming an ideal gas at 1 atm of pressure, and such assumptions may create some uncertainty for a true combustion flame. All low-frequency modes were treated as harmonic oscillators. Zero-point vibrational energy (ZPE) corrections were scaled by 0.9806.[29] To account for the thermal contribution of the radical species, a factor of RT ln 2 was added to the Thermo94 free energy corrections. All energies discussed in this paper are Gibbs free energies derived from the B3LYP/6-311+G**//B3LYP/6-31G* energies and thermal and entropic corrections as stated above, unless otherwise noted.

The CBS-QB3[30] composite method was used to recalculate the geometries and energies for the addition of O_2 to 2-oxepinoxy radical as well as the most favored pathway, to render a comparison to the energetics of our B3LYP/6-311+G**//B3LYP/6-31G* surface.

III. Results

A. Oxygen Addition to 2-Oxepinoxy Radical. The addition of O_2 to 2-oxepinoxy radical (**1**) can occur at three different positions on the 2-oxepinoxy radical ring, forming three distinctive peroxyoxepinone radicals (**1a**, **1b**, or **1c**, Figure 2), due to delocalization of the free electron within the π network of the ring carbons. Addition of O_2 to **1** can occur at the 2-, 4-, and 6-ring carbon positions (see Figure 2), numbered relative to the carbonyl carbon as position 1, moving counterclockwise (**1**). Also shown in Figure 2 are the 298 K free energies (ΔG(298 K)) for each intermediate and transition state relative to reactants at infinite separation. Each free energy of activation barrier is relative to the reactant for that individual step.

A.1. 2-Addition. Three unique transition state (TS) structures for the formation of 2-peroxyoxepinone radical **(1a)** were found.

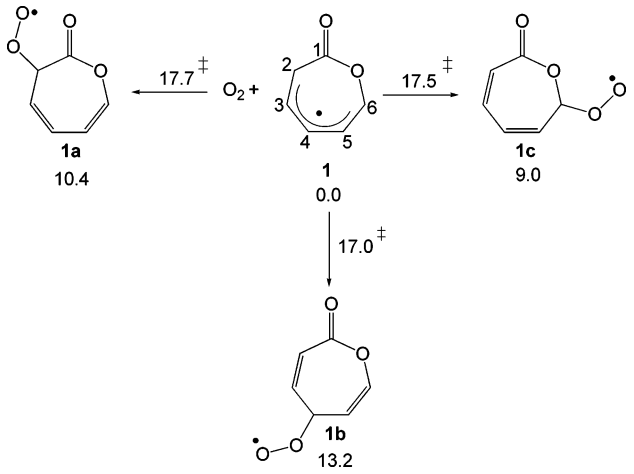

Figure 2. Reaction scheme for the addition of molecular oxygen ($^3\Sigma_g$) to 2-oxepinoxy radical (**1**). Free energies (298 K) are at the B3LYP/6-311+G**//B3LYP/6-31G* level, relative to O_2 and 2-oxepinoxy radical at infinite separation.

In each transition state, the oxygen molecule approaches perpendicular to the ring plane and differs in the orientation of the O−O bond relative to the forming C−O bond. All three TS wave functions have considerable spin contamination, giving $\langle S^2 \rangle$ values of ∼1.0, rendering the transition state barriers to be suspect. This level of spin contamination is not surprising because the separated reactants form a quartet state but the product is a doublet. Regardless, the 298 K free energy barrier ($\Delta G^{\ddagger}$(298 K)) for the lowest energy TS structure, with the O−O oxygen bond setting above the C_1-C_2 ring bond, is 17.7 kcal/mol with an $\langle S^2 \rangle$ value of 0.96, the least spin contaminated of the three TS wave functions. The 298 K reaction is endoergic by 10.4 kcal/mol with a reverse $\Delta G^{\ddagger}$(298 K) of only 7.3 kcal/mol.

A.2. 4-Addition. Two TS structures were found for addition of oxygen to the 4-carbon to form 4-peroxyoxepinone radical **(1b)**. In both transition structures, the oxygen molecule approaches perpendicular to the ring plane. In the lower energy TS, the O−O bond adds anti to the C−H bond at the 4-position whereas the higher energy structure has the O−O bond almost eclipsing the C−H bond. Spin contamination for both transition states was also significant, ($\langle S^2 \rangle \sim 1.0$). The $\Delta G^{\ddagger}$(298 K) for the lowest energy transition structure was 17.0 kcal/mol. This barrier is the lowest for molecular oxygen addition at either of the three carbon positions. A simple Hückel MO analysis for the 5-carbon ring π system for **1** would indicate that most of the electron density should be localized on the 4-carbon, allowing for the relative ease of oxygen addition. Examination of the C−C bond lengths on the ring are consistent with Hückel theory, as the two C−C bonds containing the 4-carbon are 1.40 and 1.42 Å, bond lengths intermediate between typical C−C single and double bond character. The adjacent C−C bonds have lengths of 1.38 and 1.36 Å, exhibiting more pure C═C character. Formation of **1b**, however, is endoergic by 13.2 kcal/mol and is the most unstable addition product, due to disruption of resonance interaction between the double bonds of the π system. Re-crossing back to reactants costs a mere 3.8 kcal/mol.

A.3. 6-Addition. Three transition state structures for the formation of 6-peroxyoxepinone radical **(1c)** were also found. Each TS structure has the oxygen molecule approaching perpendicular to the ring plane and differs only by a rotation of the O−O bond about the forming C−O bond. All three TS wave functions have considerable spin contamination, $\langle S^2 \rangle$ values of ∼1.0, making the TS energies to be suspect. The $\Delta G^{\ddagger}$(298 K) for the lowest energy TS, with the O−O oxygen bond residing above the C−O ring bond, is 17.5 kcal/mol with an $\langle S^2 \rangle$ value of 1.1. The reaction is endoergic by 9.0 kcal/mol, making **1c** the most stable of the peroxyoxepinone radical species. Return to reactants has a $\Delta G^{\ddagger}$(298 K) of 8.5 kcal/mol, the largest of the return barriers.

B. Reaction Mechanism and Products of Peroxyoxepinone (1a, 1b, 1c) Decomposition. Following the formation of each peroxyoxepinone radical (**1a**, **1b**, **1c**), rearrangement to several isomers leading to decomposition is possible. Five general rearrangement intermediates have been explored to include the formation of a dioxetanyl (1,2-peroxy), 1,3-peroxy, 1,4-peroxy, and an abstraction intermediate. Furthermore, scission of the peroxy O−O bond prior to decomposition was considered. Figures 3−5 show the possible decomposition pathways calculated for **1a**, **1b** and **1c**, respectively. The ΔG(298 K) energies for each intermediate relative to 2-oxepinoxy radical and $O_2(^3\Sigma_g)$ at infinite separation and $\Delta G^{\ddagger}$(298 K) for each individual step relative to the reactant(s) for that step at the B3LYP/6-311+G**//B3LYP/6-31G* level are given in each figure.

B.1. 2-Peroxyoxepinone Radical (1a). Abstraction by the peroxy group, on 2-peroxyoxepinone, of the hydrogen on the 2-carbon gives 2-hydroperoxyoxepin-1-one-2-yl radical (**2a**). The abstraction product (**2a**) is the most stable of the initial intermediates with an exoergicity of 12.4 kcal/mol relative to 2-peroxyoxepinone (**1a**). The barrier to formation of **2a** is one of the largest due to a strained four-membered ring TS geometry. Facile loss of hydroxyl radical forms oxepin-1,2-dione (**3a**). The formation of **3a** is exoergic by 25.9 kcal/mol relative to **2a**. The cumulative free energy barrier relative to **1** and O_2 is +47.7 kcal/mol. This pathway leads to a stable, closed-shell species and further decomposition of **3a** was not examined.

Isomerization of 2-peroxyoxepinone radical (**1a**) by addition of the free end of the peroxy moiety to carbon-3 forms the radical derived from 3,8,9-trioxabicyclo[5.2.0]non-4-ene-2-one (**4a**). Scission of the shared ring C−C bond of **4a** is followed by O−O bond breakage to form, in a highly exoergic process, a radical derived from 4-oxobut-1-enyl oxoacetate (**5a**). Breaking the ester carbonyl−oxygen bond of **5a** gives 1,4-but-2-enedial and 1,2-ethanedial radical (**6a**). Further decomposition of 1,2-ethanedial radical gives formyl radical and carbon monoxide (**7a**). Completion of this pathway is exoergic by 45.0 kcal/mol with a total free energy barrier of 44.6 kcal/mol. Alternatively, **5a** can cyclize and form furanyl oxoacetate radical (**8a**). After two facile bond scissions, this pathway results in the generation of furan, CO_2, and formyl radical (**10a**). The pathway from **5a** leading to **10a** has the same overall free energy barrier as the pathway leading to **7a**; however, **5a** → **8a** → **9a** → **10a** is much more thermodynamically favored with an overall exoergicity of −84.9 kcal/mol.

2-Peroxyoxepinone radical (**1a**) can rearrange to form a 1,3-peroxy bicyclic intermediate by addition of the free end of the peroxy group to carbon-4, resulting in 3,7,8-trioxabicyclo[4.2.1]-non-4-ene-3-one-9-yl radical (**11a**). Two pathways for decomposition of **11a** are considered. One is discussed here and shown in Figure 3. The second will be discussed, and shown in Figure 4, with relation to 4-peroxyoxepinone decomposition, because **11a** is also formed by rearrangement of **1b**. Decomposition of **11a** can result from breaking the bond between a bridge carbon and the 5-carbon, leaving a high-energy vinyl radical intermediate (**12a**). Subsequent loss of C_2H_2, followed by CO_2, results in CO_2, C_2H_2, and 3-oxopropanal-2-yl radical (**14a**) as products. The step from **13a** to **14a**, corresponding to loss of CO_2, is extremely exoergic (∼98 kcal/mol) and is possible to be a

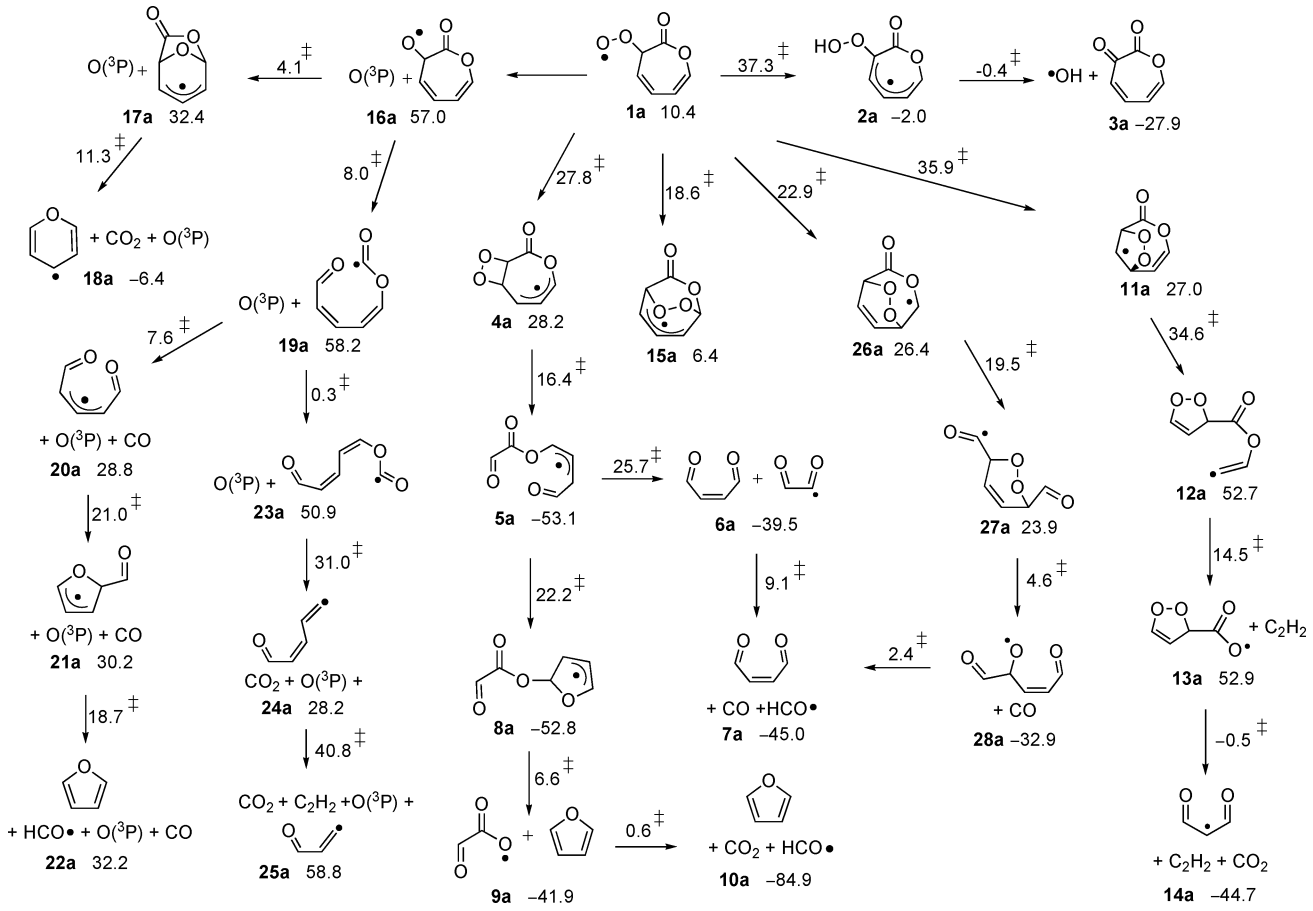

Figure 3. Unimolecular decomposition pathways of 2-peroxyoxepinone radical (**1a**). The relative free energies (kcal/mol, 298 K) at the B3LYP/6-311+G**//B3LYP/6-31G* level are shown for each intermediate relative to **1** (Figure 2), and each free energy of activation is relative to the reactant for that specific step.

barrierless reaction, given a $\Delta G^{\ddagger}$(298 K) of only −0.5 kcal/mol for the step. The overall reaction is exoergic by 44.7 kcal/mol with a free energy of activation of +61.6 kcal/mol due to the formation of **14a**.

Two 1,4-peroxy intermediates can be formed from **1a**. The formation of 2,6-peroxyoxepinone radical (**15a**) has a relatively low $\Delta G^{\ddagger}$(298 K) of 18.6 kcal/mol and is the least endoergic of the peroxy ring intermediates at ΔG(298 K) of only 6.4 kcal/mol. Decomposition of **15a** is discussed in the section for **1c** and shown in Figure 5, as 6-peroxyoxepinone radical also forms the 1,4-peroxy intermediate **15a**. Rearrangement to form 2,5-peroxyoxepinone radical (**26a**) from **1a** is also possible. Scission of the ester linkage of **26a** results in 3-formyl-6-carbonyl-1,2-oxocyclohex-4-ene radical (**27a**). Upon extrusion of CO from **27a,** the O−O ring bond can break, resulting in 5-formyl-4-oxypentenal radical (**28a**) which can easily lose the formyl group to form **7a**. This pathway has an overall $\Delta G^{\ddagger}$(298 K) of 45.9 kcal/mol due to breakage of the ester linkage to form **27a** and a ΔG(298 K) of −45.0 kcal/mol.

The final pathway examined for the decomposition of 2-peroxyoxepinone radical (**1a**) involves O−O bond scission and therefore release of an oxygen atom from the peroxy group to form 2-oxyoxepinone radical (**16a**). This reaction is analogous to the proposed mechanism for formation of phenoxy radical and oxygen atom in the high-temperature reaction between phenyl radical and molecular oxygen. A reliable TS for this O−O scission step has not been found. First-order saddle points have been located but each suffers from excess spin contamination and do not feature a normal coordinate displacement vector that connects the correct reactant/product pair. However, this **1a** to **16a** step is highly endoergic, and the TS barrier has to be at least that value. Rearrangement of **16a** by addition of the oxy moiety across the ring to the 6 carbon forms a bicyclic pyranyl lactone radical (**17a**). Liberation of CO_2 from **17a** gives pyranyl radical, CO_2, and oxygen atom (**18a**) with a total path exoergicity of −6.4 kcal/mol.

Cleavage of the C_1-C_2 bond of **16a** gives the radical derived from 5-oxopenta-*s*-*cis*-1,3-dienyl formate radical (**19a**). Two pathways for the decomposition of **19a** were considered. Extrusion of CO from **19a** results in the radical derived from 5-oxo-2-pentenal (**20a**), which can cyclize (**21a**) and then extrude formyl radical, thereby forming furan, CO, formyl radical, and oxygen atom as eventual products (**22a**). Formation of **22a** is endoergic by 31.8 kcal/mol. Alternatively, isomerization of the dienyl moiety of **19a** from a cis to a trans orientation results in 5-oxopenta-*s*-*trans*-1,3-dienyl formate radical (**23a**) with a trivial barrier of 0.3 kcal/mol. Extrusion of CO_2 from **23a** gives 5-oxopenta-*s*-*trans*-2,4-dienyl radical (**24a**), CO_2 and oxygen atom. Further decomposition via extrusion of acetylene, from **24a**, gives 3-oxo-1-propenyl radical (**25a**). Decomposition via this pathway is considerably endoergic at 298 K with a free energy of +58.8 kcal/mol. The overall activation free energy for reaction is +81.9 kcal/mol due to the loss of CO_2 from **23a** to **24a**. If it is assumed that the addition of O(^{3}P) to **16a**, the reverse of O−O scission, is barrierless, then the $\Delta G^{\ddagger}$(298 K) to form **16a** would be ∼60 kcal/mol and would not be the rate-limiting step for pathways passing through **16a**.

The rotation of 5-oxopenta-*s*-*trans*-2,4-dienyl radical (**24a**), resulting in the 5-oxopenta-*s*-*cis*-2,4-dienyl radical rotamer, is

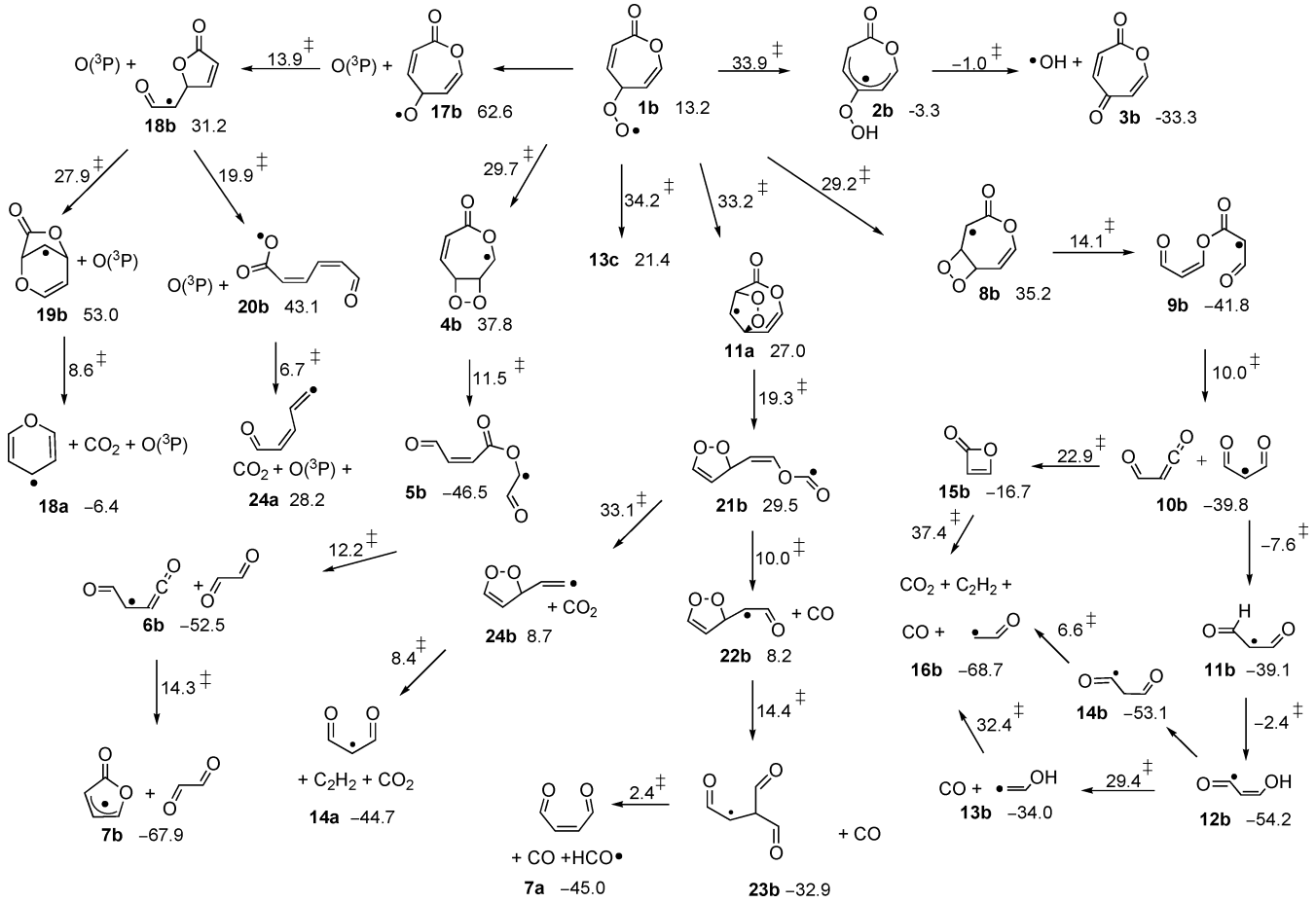

Figure 4. Unimolecular decomposition pathways of 4-peroxyoxepinone radical (**1b**). The relative free energies (kcal/mol, 298 K) at the B3LYP/6-311+G**//B3LYP/6-31G* level are shown for each intermediate relative to **1** (Figure 2), and each free energy of activation is relative to the reactant for that specific step.

an intermediate in a previous study by this group of the unimolecular decomposition of 2-oxepinoxy radical (**1**).[31] Fadden et al. showed that 5-oxopenta-*s*-*cis*-2,4-dienyl radical can possibly rearrange to form pyranyl radical and 2-cyclopentenone-1-yl radical as well as decompose to vinyl radical, acetylene, and two CO molecules. The thermodynamically most favorable products of those unimolecular "Fadden" pathways is 2-cyclopentenone-1-yl radical with a ΔG(298 K) of −50.5 kcal/mol relative to the cis isomer of **24a**. Pyranyl radical has a ΔG(298 K) of −38.7 kcal/mol, whereas the decomposition products have a ΔG(298 K) of +15.4 kcal/mol relative to the cis isomer of **24a**. Formation of all of the "Fadden" products are more exoergic than formation of **25a** via Figure 3.

B.2. 4-Peroxyoxepinone Radical (1b). The pathways considered for the decomposition of 4-peroxyoxepinone (**1b**) are given in Figure 4. Abstraction of the hydrogen on carbon-4 of **1b** gives 4-hydroperoxyoxepin-1-one-4-yl radical (**2b**). Loss of hydroxyl radical forms oxepin-1,4-dione (**3b**) and proceeds without a barrier. The formation of **3b** is exoergic at 298 K by 33.3 kcal/mol relative to reactants with an activation barrier of +47.1 kcal/mol, owing to the strained hydrogen-abstraction TS. This pathway leads to a stable closed-shell species, and the further decomposition of **3b** was not considered.

Addition of the free end of the peroxy moiety of **1b** to carbon-5 forms one possible dioxetanyl intermediate, 3,8,9-trioxabicyclo[5.2.0]non-4-en-3-one-2-yl radical (**4b**). Scission of the dioxetane's O−O bond results in the immediate cleavage of the C−C ring fusion to yield an acyclic radical derived from 2-oxoethyl-4-oxobutan-2-enoate (**5b**). Scission of the C−O bond of the ester linkage leads to 4-oxobut-3-enal-2-yl radical and *trans*-ethanedial (**6b**). Rotation around C_1-C_2 bond of **6b** results in the formation of γ-butyrolactonyl radical and *trans*-ethanedial (**7b**). The overall pathway is exoergic having a 298 K free energy of reaction of −67.9 kcal/mol, and an overall $\Delta G^{\ddagger}$(298 K) of +49.3 kcal/mol, due to the formation of **5b** and endoergicity of **4b** formation.

Formation of another dioxetanyl intermediate is possible via the addition of the free end of the peroxy moiety of 4-peroxyoxepinone radical (**1b**) to carbon-3 forming 4,8,9-trioxabicyclo-[5.2.0]non-4-en-3-one-2-yl radical (**8b**). Cleavage of the C−C fusion is followed by concomitant breakage of the dioxetane's O−O bond, in a process with a ΔG(298 K) of −78 kcal/mol, thereby forming 3-oxopropenyl 3-oxopropenoate radical (**9b**). Scission of the ester's C−O linkage results in the formation of two intermediates, 3-oxopropenal and propan-1,3-dial-2-yl radical (**10b**). Decomposition pathways of both **10b** species have been calculated, each yielding 2-oxoethanyl radical, carbon monoxide, carbon dioxide, and acetylene (**16b**). The energies listed in Figure 4 for these separate branching paths correspond to that of the intermediate shown and the individual component of **10b**. 3-Oxopropenal can cyclize to form β-propenolactone (**15b**), which can break apart to form acetylene and carbon dioxide. Decomposition of propane-1,3-dial-2-yl radical is initiated by bond rotation and a 1,4-hydrogen-atom transfer resulting in 3-hydroxy-1-oxoprop-2-eneyl radical (**12b**). From **12b**, two pathways have been considered. Bond scission gives CO and 2-hydroxyethenyl radical (**13b**). 2-Hydroxyethenyl radical can undergo a 1,3-hydrogen shift to form 2-oxoethanyl

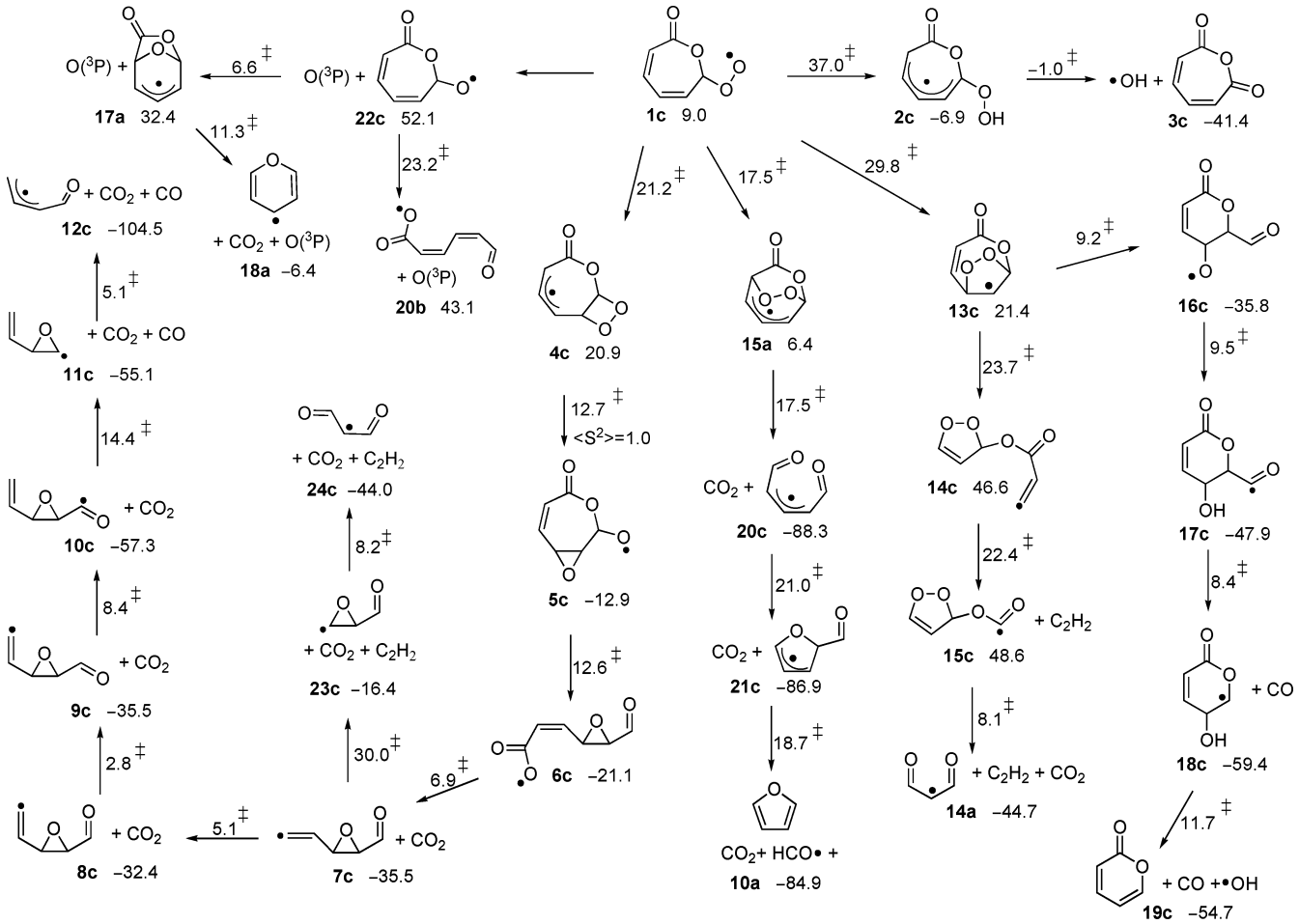

Figure 5. Unimolecular decomposition pathways of 6-peroxyoxepinone radical (**1c**). The relative free energies (kcal/mol, 298 K) at the B3LYP/6-311+G**//B3LYP/6-31G* level are shown for each intermediate relative to **1** (Figure 2), and each free energy of activation is relative to the reactant for that specific step.

radical (**16b**). Rearrangement to form the tautomer of **12b** (**14b**) affords a more facile CO extrusion to give the same products. The overall free energy of activation for this pathway is +49.3 kcal/mol, due to the formation of **9b**, and is exoergic by 68.7 kcal/mol.

Two 1,3-peroxy intermediates resulting from the rearrangement of **1b** include **11a**, which was introduced as an intermediate for **1a** decomposition, and 2,7,8-trioxabicyclo[4.2.1]non-4-ene-3-one-9-yl radical (**13c**), an intermediate also generated by 6-peroxyoxepinone radical (**1c**). One pathway for decomposition of **11a** was discussed in the previous section, and a second set will be discussed here. (The decomposition of **13c** will be presented within the discussion of the 6-peroxyoxepinone radical (**1c**) pathways, shown in Figure 5.) Bond scission of C_1-C_2 bond of **11a** results in the radical derived from 2-(3H-[1,2]-dioxol-3-yl)-vinyl formate (**21b**). Expulsion of CO has a relatively low free energy barrier at 298 K of 10 kcal/mol, yielding **22b**. Scission of the O−O bond of **22b** causes a rearrangement of the carbon backbone of **22b**, forming a transitory 2,3-diformyl-1-oxycyclopropane radical intermediate that undergoes ring opening, yielding 3,3-diformylpropanal radical (**23b**). Facile loss of one of the formyl groups at the 3-position of **23b** gives 1,4-butendial, CO, and formyl radical (**7a**). This pathway has a ΔG(298 K) of −45.0 kcal/mol. The largest barrier for this pathway results from formation of **21b** from **11a**. Instead, if **21b** extrudes CO_2 as an initial fragmentation, then **24b** can lose acetylene, which is followed by ring opening to yield 3-oxopropenal radical, CO_2, and C_2H_2 (**14a**). The CO_2 extrusion pathway has a similar exoergicity, at 298 K, to the CO extrusion pathway ($\Delta G = -44.7$ kcal/mol). The largest barrier for this path comes from CO_2 extrusion with a 298 K free energy barrier of +62.4 kcal/mol.

The final pathways calculated for **1b** decomposition include the O−O peroxy bond scission intermediate **17b**. Formation of **17b** is endoergic at 298 K by +62.6 kcal/mol, and the barrier for O−O bond scission has not been determined because a legitimate TS has not been found. Further decomposition of **17b** can be initiated by attack at the carbonyl carbon by the oxy moiety causing simultaneous breakage of the C−O ester linkage resulting in a ring contraction (**18b)**. From **18b**, two decomposition pathways have been examined. If the exocyclic oxygen of **18b** adds to the ring carbon α to the carbonyl carbon, the bicyclic structure **19b** is generated, which can easily eliminate CO_2 to yield pyranyl radical **18a.** If the ring C−O bond of **18b** is broken, the radical derived from 1,6-oxohex-2,4-en-1-oxy radical (**20b**) is formed, which can easily extrude CO_2, thereby generating **24a**. As shown for the 2-peroxyoxepinone radical (**1a**) (Figure 2), **24a** can decompose to form C_2H_2, CO_2, $O(^3P)$, and 3-oxo-1-propenyl radical (**25a**). Bond rotation of **24a** allows an intersection with pathways for the unimolecular decomposition of 2-oxepinoxy,[31] as mentioned in the previous section. Neither of the oxygen atom extrusion products are the most thermodynamically favored at low temperatures. Formation of pyranyl radical (**18a**) is exoergic only by −6.4 kcal/mol, and formation of **25a** is endoergic by 58.8 kcal/mol. The 298 K

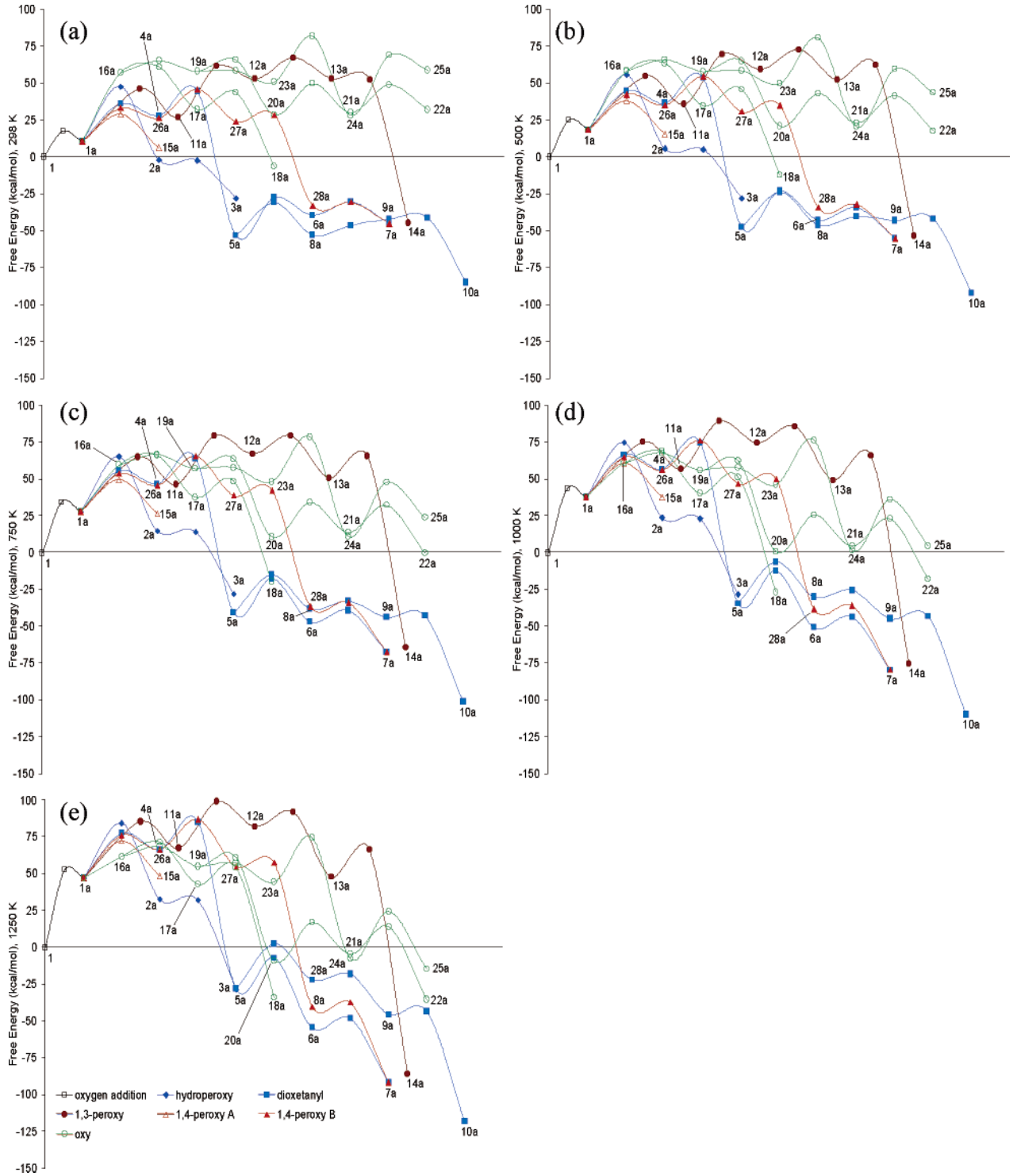

Figure 6. Unimolecular decomposition pathways of 2-peroxyoxepinone radical (**1a**) from 298 (a), 500 (b), 750 (c), 1000 (d), and 1250 (e) K using the mechanistic pathways shown in Figure 3. The relative Gibbs free energies at the B3LYP/6-311+G**//B3LYP/6-31G* level are shown relative to 2-oxepinoxy radical and $O_2(^3\Sigma_g)$ at infinite separation.

free energy barrier for both pathways is at least 76.5 kcal/mol due to the formation of **18b** from **17b**.

B.3. 6-Peroxyoxepinone Radical (1c). The pathways considered for the decomposition of 6-peroxyoxepinone radical (**1c**) are shown in Figure 5. Abstraction of the hydrogen on carbon-6 by the terminal oxygen of the peroxy moiety gives 6-hydroperoxyoxepin-1-one-6-yl radical (**2c**). Barrierless fragmentation of hydroxyl radical forms oxepin-1,6-dione (**3c**). The formation of **3c** is exoergic at 298 K by 41.4 kcal/mol relative to 2-oxepinoxy and oxygen with a free energy barrier of +46.0 kcal/mol due to the tight H-atom-abstraction TS geometry. This pathway leads to a stable closed-shell species and further decomposition steps from **3c** were not examined.

Ring closure of 6-peroxyoxepinone radical (**1c**) by addition of the free end of the peroxy moiety to carbon-5 forms 3,8,9-trioxabicyclo[5.2.0]non-4-ene-2-one-3-yl radical (**4c**). A greater degree of delocalization for the unpaired electron in **4c** makes it the most stable dioxetanyl intermediate considered here. Cleavage of the dioxetane's O−O bond leads to the formation of a bicyclic oxiranyl structure, 2-oxy-3,8-dioxabicyclo[5.1.0]-oct-5-en-4-one radical (**5c**). The transition state leading to formation of **5c** from **4c** suffers from excess spin contamination

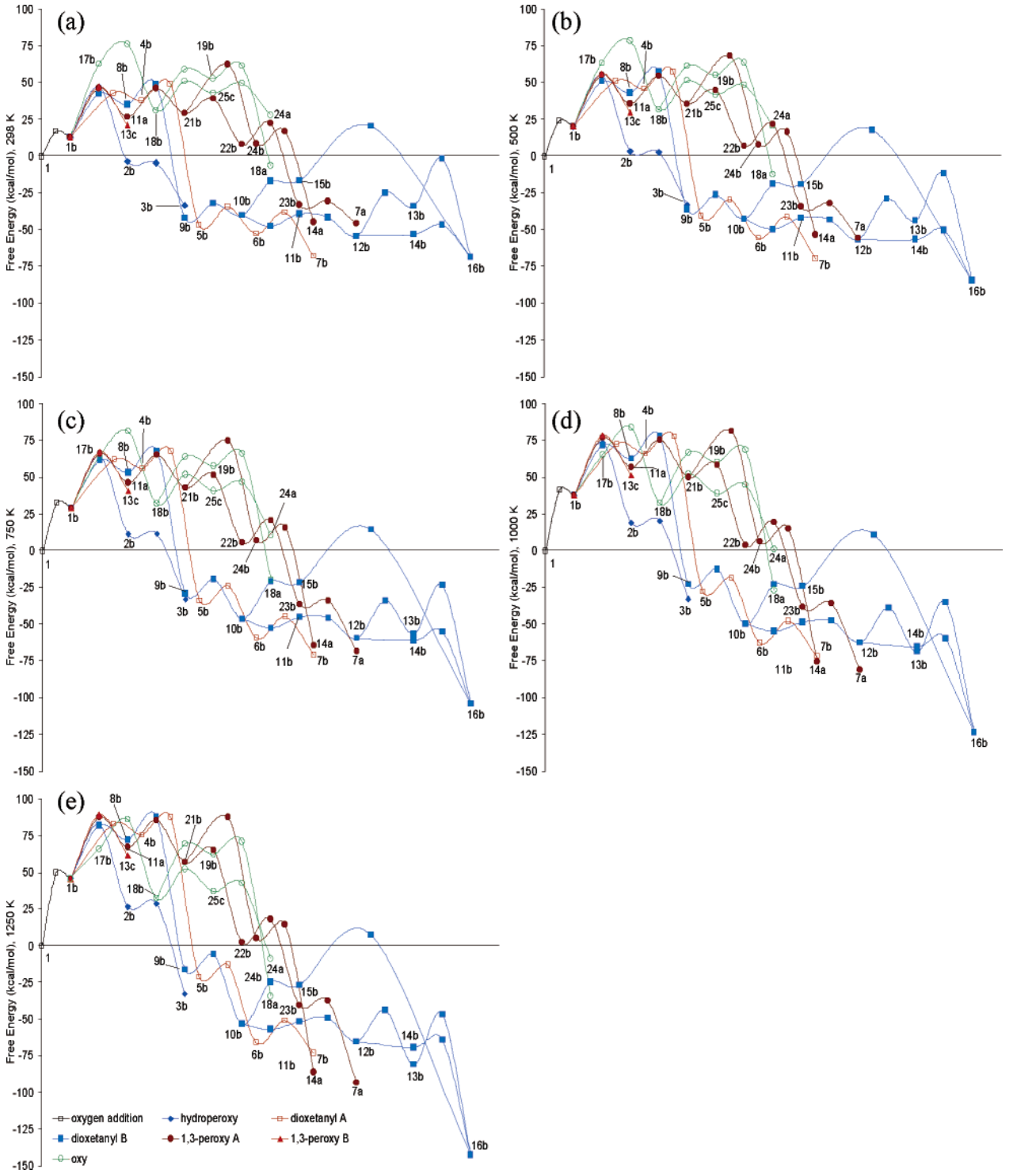

Figure 7. Unimolecular decomposition pathways of 4-peroxyoxepinone radical (**1b**) from 298 (a), 500 (b), 750 (c), 1000 (d), and 1250 (e) K using the mechanistic pathways shown in Figure 4. The relative Gibbs free energies at the B3LYP/6-311+G**//B3LYP/6-31G* level are shown relative to 2-oxepinoxy radical and $O_2(^3\Sigma_g)$ at infinite separation.

($\langle S^2 \rangle = 1.0$), rendering it to be suspect. Breaking the C−O ester linkage of **5c** opens the ring of the oxepinone, while the epoxide ring is maintained, to give 3-(3-formyloxiranyl)acrylic carboxy radical (**6c**), which can easily eliminate CO_2 and form **7c**. Following two bond rotations, via **8c** and **9c**, a 1,5-hydrogen shift yielding **10c** allows for the extrusion of CO to form 1,2-epoxy-3-buten-1-yl radical (**11c**). Facile opening of the epoxide ring gives 1-oxo-3-buten-2-yl radical along with CO_2 and CO (**12c**). Formation of **12c** is extremely exoergic due to the relief of ring strain and increased delocalization. The overall process is exoergic at 298 K by −104.5 kcal/mol with an overall 298 K activation free energy of +33.6 kcal/mol relative to reactants (**1**), due to the barrier for the **4c** → **5c** transformation. Additionally, expulsion of acetylene from **7c** gives formyloxiranyl radical (**23c**), which can undergo facile ring opening to form an *s-trans* isomer of **14a**, *s-trans*-3-oxa-propanal radical (**24c**).

6-Peroxyoxepinone radical (**1c**) can undergo ring closure to form a 1,3-peroxy intermediate by addition of the free end of the peroxy group to carbon-4 to give 2,8,9-trioxabicyclo[4.2.1]-non-4-ene-3-one-9-yl radical (**13c**). The 1,3-peroxy intermediate (**13c**) is also formed, in a similar fashion, from **1b**. Bond scission

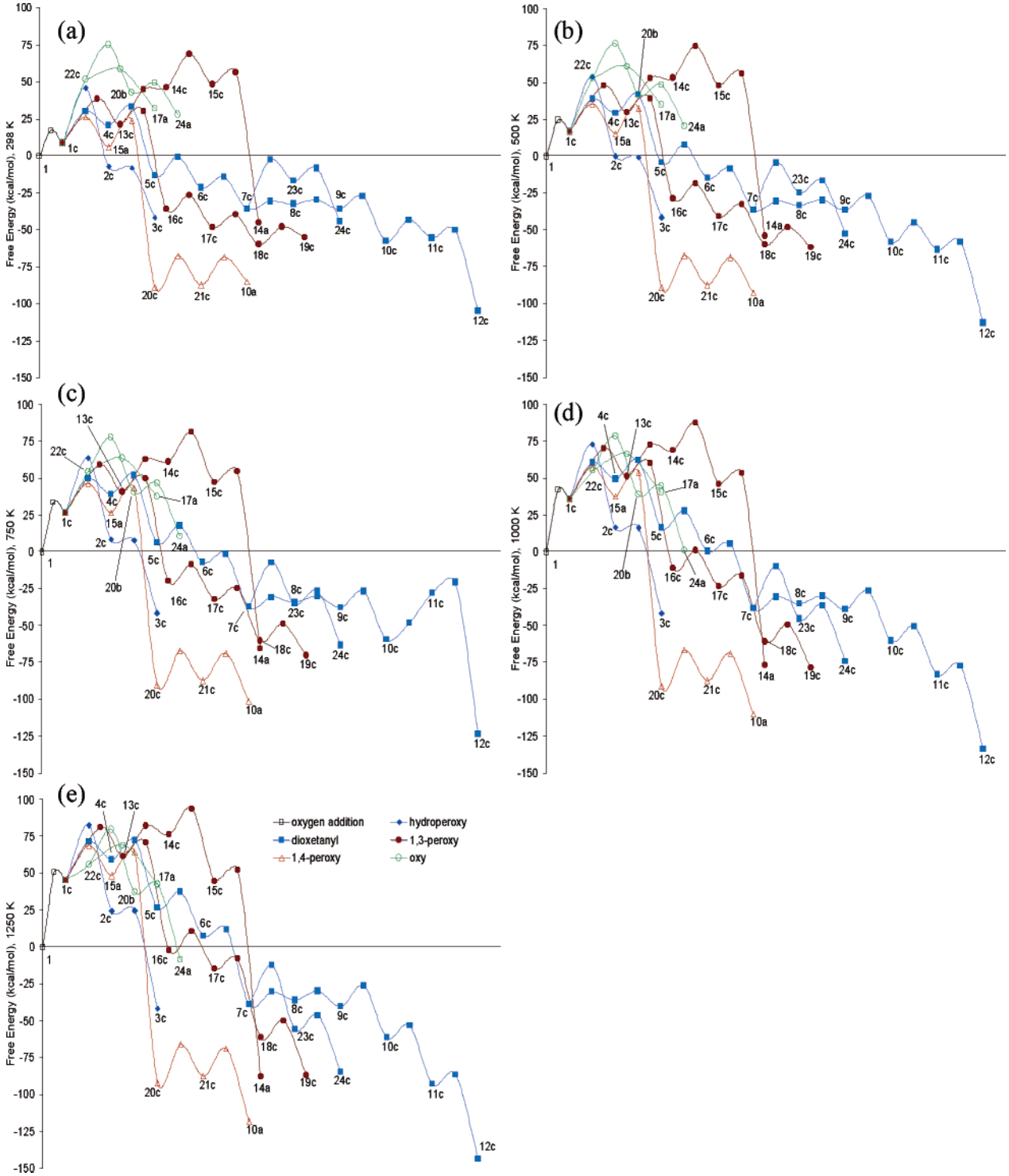

Figure 8. Unimolecular decomposition pathways of 6-peroxyoxepinone radical (**1c**) from 298 (a), 500 (b), 750 (c), 1000 (d), and 1250 (e) K using the mechanistic pathways shown in Figure 5. The relative Gibbs free energies at the B3LYP/6-311+G**//B3LYP/6-31G* level are shown relative to 2-oxepinoxy radical and $O_2(^3\Sigma_g)$ at infinite separation.

of the C_2-C_3 bond of **13c** results in the radical derived from 3*H*-[1,2]dioxol-3-ylacrylate (**14c**). Loss of C_2H_2 (**15c**) followed by CO_2 results in 3-oxopropanal-2-yl radical (**14a**). The barrier for loss of CO_2 from **15c** → **14a** is very small. This may be attributed to the exoergicity of the step that is aided by opening of the ring ($\Delta G(298\ K) = -93.3$ kcal/mol). The overall pathway is exoergic at 298 K by −44.7 kcal/mol with a 298 K free energy of activation of 69.0 kcal/mol due to the barrier to expel C_2H_2.

Alternatively, upon scission of the C_6-O bond on the oxepinone ring of **13c**, the oxygen may form a bond with C_5, and the peroxy bond is broken to yield 2-formyl-6-keto-3-oxy-1-oxacyclohex-4-ene radical (**16c**). Following an exocyclic 1,4-hydrogen transfer from the formyl group to the oxy moiety of **16c** to generate **17c**, CO can be extruded (**18c**), allowing for further fragmentation of OH radical, resulting in 2*H*-pyran-2-one (**19c**). The overall pathway is exoergic at 298 K by 54.7 kcal/mol with a 298 K free energy of activation of 38.8 kcal/mol due to the formation of the 1,3-peroxy intermediate (**13c**).

6-Peroxyoxepinone radical (**1c**) can also rearrange to form the 1,4-peroxy intermediate **15a** by addition of the free end of the peroxy moiety to carbon-2. This intermediate is also formed via rearrangement of 2-peroxyoxepinone radical (**1a**) (Figure

TABLE 1: Relative Gibbs Free Energies for All Intermediates and Transition States (298−1250 K) at the B3LYP/6-311+G// B3LYP/6-31G* Level Related to 1a Decomposition**

structure[a]	E[b] (hartrees/part)	ΔG(298 K) (kcal/mol)	ΔG(500 K) (kcal/mol)	ΔG(750 K) (kcal/mol)	ΔG(1000 K) (kcal/mol)	ΔG(1250 K) (kcal/mol)	$\langle S^2 \rangle$	other (PG, ES, N_{imag})[c]
phenyl + 2(O_2)	−532.36918	80.4	73.3	64.7	56.3	48.0	0.76	C_{2v}, $^2A_1$, 0
1[d]	−532.51741	0.0	0.0	0.0	0.0	0.0	0.78	C_1, −, 0
TS (1−1a)	−532.50807	17.7	25.2	34.4	43.6	52.7	0.96	C_1, −, 1
1a	−532.52289	10.4	18.4	28.1	37.6	47.0	0.75	C_1, −, 0
TS (1a−2a)	−532.45727	47.7	55.6	65.3	74.9	84.4	0.78	C_1, −, 1
2a	−532.54115	−2.0	5.7	14.9	23.8	32.6	0.78	C_1, −, 0
TS (2a−3a)	−532.53925	−2.3	5.1	14.2	23.2	32.1	0.81	C_1, −, 1
3a[e]	−532.56069	−27.9	−27.9	−28.0	−28.3	−28.5	0.00	C_1, −, 0
TS (1a−4a)	−532.48181	36.2	44.9	55.8	66.7	77.6	0.78	C_1, −, 1
4a	−532.49525	28.2	36.5	46.7	56.7	66.6	0.78	C_1, −, 0
TS (4a−5a)	−532.46631	44.6	53.3	64.0	74.7	85.2	0.80	C_1, −, 1
5a	−532.61728	−53.1	−47.5	−40.8	−34.3	−28.0	0.78	C_1, −, 0
TS (5a−6a)	−532.57070	−27.3	−22.8	−17.5	−12.2	−7.0	0.76	C_1, −, 1
6a	−532.57062	−39.5	−42.7	−46.7	−50.6	−54.5	0.76	C_s, $^2A''$, 0; C_2, ^1A, 0
TS (6a−7a)	−532.55145	−30.4	−34.3	−39.1	−43.7	−48.2	0.76	C_2, ^1A, 0
7a	−532.55835	−45.0	−55.0	−67.4	−79.5	−91.4	0.00	C_1, −, 0
TS (5a−8a)	−532.58376	−30.9	−23.7	−14.9	−6.2	2.5	0.76	C_1, −, 1
8a	−532.62024	−52.8	−46.1	−37.9	−29.9	−22.0	0.77	C_1, −, 0
TS (8a−9a)	−532.60612	−46.3	−40.2	−32.8	−25.4	−18.1	0.76	C_1, −, 1
9a[f]	−532.58120	−41.9	−42.8	−43.8	−44.6	−45.5	0.76	C_1, −, 0
TS (9a−10a)[f]	−532.57821	−41.3	−42.0	−42.7	−43.2	−43.5	0.75	C_1, −, 1
10a[g]	−532.63164	−84.9	−92.3	−101.1	−109.8	−118.1	0.75	C_{2v}, $^1A_1$, 0
TS (1a−11a)	−532.46386	46.3	54.6	64.9	75.2	85.4	0.80	C_1, −, 1
11a	−532.49746	27.0	35.8	46.5	57.0	67.4	0.75	C_1, −, 0
TS (11a−12a)	−532.43741	61.6	69.7	79.6	89.3	99.0	0.78	C_1, −, 1
12a	−532.44987	52.7	59.3	67.1	74.7	82.1	0.76	C_1, −, 0
TS (12a−13a)	−532.42110	67.2	72.8	79.4	85.7	91.9	0.77	C_1, −, 1
13a[h]	−532.39614	52.9	52.1	50.8	49.3	47.8	0.76	C_1, −, 0
TS (13a−14a)[h]	−532.39573	52.3	62.3	65.5	66.0	66.3	0.76	C_1, −, 1
14a[i]	−532.53108	−44.7	−53.4	−64.4	−75.3	−86.0	0.78	C_{2v}, $^2B_1$, 0
TS (1a−15a)	−532.49401	29.0	38.2	49.6	61.0	72.3	0.80	C_1, −, 1
15a	−532.53186	6.4	15.5	26.7	37.8	48.6	0.78	C_1, −, 0
TS (1a−16a)	*p*							
16a[j]	−532.40029	57.1	58.3	59.6	60.7	61.7	0.75	C_1, −, 0
TS (16a−17a)[j]	−532.39419	61.1	63.4	66.2	68.9	71.6	0.77	C_1, −, 1
17a[j]	−532.44296	32.4	34.8	37.7	40.4	43.0	0.78	C_1, −, 0
TS (17a−18a)[j]	−532.42239	43.7	45.9	48.6	51.3	54.0	0.77	C_1, −, 1
18a[k]	−532.48249	−6.4	−12.2	−19.5	−26.8	−34.0	0.78	C_{2v}, $^2B_1$, 0
TS (16a−19a)[j]	−532.38418	65.1	65.9	66.9	67.8	68.6	0.76	C_1, −, 1
19a[j]	−532.39411	58.2	57.8	57.0	56.1	55.0	0.75	C_1, −, 0
TS (19a−20a)[j]	−532.37773	65.8	65.0	63.7	62.4	61.0	0.78	C_1, −, 1
20a[l]	−532.41811	28.8	20.9	10.9	0.8	−9.3	0.79	C_2, ^2A, 0
TS (20a−21a)[l]	−532.38547	49.7	42.8	34.1	25.5	17.1	0.76	C_1, −, 1
21a[l]	−532.41807	30.2	23.0	13.9	4.7	−4.5	0.77	C_1, −, 0
TS (21a−22a)[l]	−532.38567	48.9	41.5	32.3	23.1	14.0	0.77	C_1, −, 1
22a[m]	−532.39388	32.2	17.7	−0.2	−17.8	−35.3	0.75	C_{2v}, $^1A_1$, 0
TS (19a−23a)[j]	−532.39262	58.4	58.3	58.0	57.7	57.3	0.76	C_1, −, 1
23a[j]	−532.40440	50.9	49.8	48.2	46.5	44.5	0.75	C_1, −, 0
TS (23a−24a)[j]	−532.35038	81.9	80.6	78.6	76.5	74.4	0.76	C_1, −, 1
24a[k]	−532.42135	28.2	20.5	11.2	1.8	−7.6	0.77	C_1, −, 0
TS (24a−25a)[k]	−532.34789	69.0	59.5	47.8	36.1	24.5	0.78	C_1, −, 1
25a[n]	−532.31748	58.8	43.4	24.0	4.7	−14.5	0.76	C_1, −, 0
TS (1a−26a)	−532.48693	33.2	42.4	53.7	65.0	76.2	0.77	C_1, −, 1
26a	−532.49847	26.4	35.1	45.8	56.3	66.6	0.76	C_1, −, 0
TS (26a−27a)	−532.46471	45.9	54.6	65.5	76.2	86.9	0.76	C_1, −, 1
27a	−532.49695	23.9	30.7	38.9	46.9	54.8	0.75	C_1, −, 0
TS (27a−28a)	−532.48577	28.5	34.8	42.4	50.0	57.4	0.77	C_1, −, 1
28a[o]	−532.56351	−32.9	−34.2	−36.2	−38.2	−40.2	0.75	C_1, −, 0
TS (28a−7a)[o]	−532.55745	−30.5	−31.9	−33.8	−35.6	−37.3	0.76	C_1, −, 1

[a] See Figure 3 for structures. [b] Bottom-of-the-well energy. [c] Point group (PG), electronic state (ES), number of imaginary vibrational frequencies (N_{imag}). [d] E and $\Delta G(T)$ values include E and $G(T)$ of O_2. [e] E and $\Delta G(T)$ values include E and $G(T)$ of OH. [f] E and $\Delta G(T)$ values include E and $G(T)$ of furan. [g] E and $\Delta G(T)$ values include E and $G(T)$ of furan, CO_2, and formyl radical. [h] E and $\Delta G(T)$ values include E and $G(T)$ of C_2H_2. [i] E and $\Delta G(T)$ values include E and $G(T)$ of CO_2 and C_2H_2. [j] E and $\Delta G(T)$ values include E and $G(T)$ of $O(^3P)$. [k] E and $\Delta G(T)$ values include E and $G(T)$ of CO_2 and $O(^3P)$. [l] E and $\Delta G(T)$ values include E and $G(T)$ of CO and $O(^3P)$. [m] E and $\Delta G(T)$ values include E and $G(T)$ of furan, CO, $O(^3P)$, and formyl radical. [n] E and $\Delta G(T)$ values include E and $G(T)$ of CO_2, $O(^3P)$, and C_2H_2. [o] E and $\Delta G(T)$ values include E and $G(T)$ of CO. [p] A reliable transition state was not found for this process.

3). Loss of CO_2 from **15a,** by breaking the C_6−O oxepinone bond, results in simultaneous scission of the peroxy O−O bond to give 5-oxo-3-pentenal radical (**20c**). Further, decomposition of **20c** can proceed by the same mechanism as that for decomposition from **20a** to **22a** (cyclization followed by formyl extrusion, **20c** to **10a**, Figure 3). Unlike the **20a** to **22a** steps, however, the **20c** to **10a** intermediates have a thermodynamically favorable 298 K free energy relative to 2-oxepinoxy radical and oxygen. This pathway is highly exoergic at 298 K at −84.9 kcal/mol with a 298 K free energy barrier of 26.5 kcal/mol resulting from the formation of **15a**. This pathway has the lowest 298 K free energy barrier of all examined steps.

TABLE 2: Relative Gibbs Free Energies for All Intermediates and Transition States (298−1250 K) at the B3LYP/6-311+G// B3LYP/6-31G* Level Related to 1b Decomposition**

structure[a]	E^b (hartrees/part)	ΔG(298 K) (kcal/mol)	ΔG(500 K) (kcal/mol)	ΔG(750 K) (kcal/mol)	ΔG(1000 K) (kcal/mol)	ΔG(1250 K) (kcal/mol)	$\langle S^2 \rangle$	other (PG, ES, N_{imag})[c]
TS (1−1b)	−532.50851	17.0	24.0	32.7	41.4	50.0	0.94	C_1, −, 1
1b	−532.51691	13.2	20.4	29.1	37.6	46.1	0.75	C_1, −, 0
TS (1b−2b)	−532.45786	47.2	54.9	64.3	73.6	82.8	0.77	C_1, −, 1
2b	−532.54148	−3.3	3.4	11.4	19.2	26.8	0.77	C_1, −, 0
TS (2b−3b)	−532.54198	−4.3	2.8	11.6	20.3	28.8	0.79	C_1, −, 1
3b[d]	−532.57036	−33.3	−33.0	−32.8	−32.7	−32.6	0	C_1, −, 0
TS (1b−4b)	−532.47045	42.9	51.4	62.0	72.6	83.1	0.77	C_1, −, 1
4b	−532.47919	37.8	46.1	56.2	66.1	75.9	0.75	C_1, −, 0
TS (4b−5b)	−532.45734	49.3	57.6	67.7	77.8	87.8	0.90	C_1, −, 1
5b	−532.60706	−46.5	−40.8	−34.0	−27.5	−21.1	0.76	C_1, −, 0
TS (5b−6b)	−532.58222	−34.2	−29.4	−23.8	−18.2	−12.8	0.77	C_1, −, 1
6b[e]	−532.59294	−52.5	−55.7	−59.2	−62.6	−66.0	0.77	C_{2h}, ^1A_g, 0; C_s, $^2A''$, 0
TS (6b−7b)[e]	−532.56801	−38.2	−41.4	−44.7	−47.9	−50.9	0.76	C_1, −, 1
7b[e]	−532.62256	−67.9	−69.4	−70.6	−71.8	−72.9	0.77	C_1, −, 0
TS (1b−8b)	−532.47086	42.4	50.9	61.4	71.8	82.2	0.78	C_1, −, 1
8b	−532.48332	35.2	43.2	53.1	62.8	72.3	0.76	C_1, −, 0
TS (8b−9b)	−532.45816	49.2	57.6	67.9	78.1	88.2	0.78	C_1, −, 1
9b	−532.59941	−41.8	−36.1	−29.3	−22.6	−16.2	0.77	C_1, −, 0
TS (9b−10b)	−532.58112	−31.9	−26.1	−19.2	−12.4	−5.6	0.77	C_1, −, 1
10b	−532.57167	−39.8	−42.7	−46.2	−49.7	−53.1	0.76	C_s, $^1A'$, 0; C_{2v}, $^2B_1$, 0
TS (10b−11b)[f]	−532.58372	−47.4	−49.6	−52.2	−54.6	−56.9	0.77	C_1, −, 1
11b[f]	−532.57139	−39.1	−41.8	−45.1	−48.3	−51.5	0.78	C_1, −, 0
TS (11b−12b)[f]	−532.57281	−41.5	−43.3	−45.4	−47.4	−49.2	0.76	C_1, −, 1
12b[f]	−532.59788	−54.2	−56.5	−59.4	−62.3	−65.1	0.75	C_1, −, 0
TS (12b−13b)[f]	−532.54312	−24.8	−28.8	−33.9	−38.9	−43.8	0.76	C_s, $^2A''$, 0
13b[g]	−532.54207	−34.0	−43.9	−56.4	−68.7	−80.8	0.76	C_s, $^2A''$, 0
TS (13b−16b)[g]	−532.48523	−1.6	−11.4	−23.4	−35.2	−46.7	0.76	C_1, −, 1
14b[f]	−532.59198	−53.1	−56.5	−60.8	−65.1	−69.3	0.75	C_1, −, 0
TS (14b−16b)[f]	−532.57817	−46.5	−50.3	−55.0	−59.5	−63.9	0.77	C_1, −, 1
TS (10b−15b)[h]	−532.53593	−17.3	−19.4	−21.8	−24.1	−26.2	0	C_1, −, 1
15b[h]	−532.54824	−16.7	−18.8	−21.5	−24.1	−26.7	0	C_1, −, 0
TS (15b−16b)[h]	−532.47124	20.3	17.2	13.4	9.6	6.0	0	C_1, −, 1
16b[i]	−532.54899	−68.7	−84.4	−104.0	−123.4	−142.5	0.77	C_1, −, 0
TS (1b−17b)	*l*							
17b[j]	−532.39077	62.6	63.6	64.6	65.3	66.0	0.76	C_1, −, 0
TS (17b−18b)[j]	−532.36886	76.5	78.7	81.3	83.8	86.3	0.76	C_1, −, 1
18b[j]	−532.43907	31.2	31.7	32.1	32.3	32.3	0.77	C_1, −, 0
TS (18b−19b)[j]	−532.39713	59.2	61.4	64.1	66.8	69.5	0.77	C_1, −, 1
19b[j]	−532.40935	53.0	55.2	57.8	60.2	62.5	0.75	C_1, −, 0
TS (19b−18a)[j]	−532.39317	61.6	63.7	66.2	68.6	71.1	0.77	C_1, −, 1
TS (18b−20b)[j]	−532.40485	51.1	51.5	51.9	52.2	52.5	0.78	C_1, −, 1
20b[j]	−532.41667	43.1	42.1	40.7	39.1	37.3	0.76	C_1, −, 0
TS (20b−24a)[j]	−532.40230	49.7	48.5	46.6	44.7	42.7	0.76	C_1, −, 1
TS (1b−11a)	−532.46518	46.4	55.2	66.1	77.0	87.9	0.81	C_1, −, 1
TS (11a−21b)	−532.46387	46.34	54.73	65.11	75.42	85.67	0.78	C_1, −, 1
21b	−532.48731	29.5	35.6	42.9	50.1	57.0	0.75	C_1, −, 0
TS (21b−22b)	−532.46737	39.3	45.0	51.8	58.5	65.1	0.77	C_1, −, 1
22b[k]	−532.49938	8.2	7.1	5.6	4.1	2.5	0.77	C_1, −, 0
TS (22b−23b)[k]	−532.47251	22.6	21.8	20.6	19.5	18.4	0.89	C_1, −, 1
23b[k]	−532.60598	−59.6	−61.4	−63.7	−66.1	−68.5	0.77	C_1, −, 0
TS (23b−7a)[k]	−532.56878	−39.8	−42.8	−46.5	−50.2	−53.9	0.77	C_1, −, 1
TS (1b−13c)	−532.46387	47.3	56.3	67.4	78.4	89.4	0.79	C_1, −, 1

[a] See Figure 4 for structures. [b] Bottom-of-the-well energy. [c] Point group (PG), electronic state (ES), number of imaginary vibrational frequencies (N_{imag}). [d] E and $\Delta G(T)$ values include E and $G(T)$ of OH. [e] E and $\Delta G(T)$ values include E and $G(T)$ of *trans*-glyoxal. [f] E and $\Delta G(T)$ values include E and $G(T)$ of formylketene. [g] E and $\Delta G(T)$ values include E and $G(T)$ of CO and formylketene. [h] E and $\Delta G(T)$ values include E and $G(T)$ of 2-malonaldehyde radical. [i] E and $\Delta G(T)$ values include E and $G(T)$ of CO, CO_2, and C_2H_2. [j] E and $\Delta G(T)$ values include E and $G(T)$ of $O(^3P)$. [k] E and $\Delta G(T)$ values include E and $G(T)$ of CO. [l] A reliable transition state was not found for this process.

The final pathways examined for the decomposition of 6-peroxyoxepinone radical (**1c**) involve the release of an oxygen atom from the peroxy group to form 6-oxyoxepinone radical (**22c**). From **22c,** two possible pathways have been calculated. Rearrangement, by addition of the oxy moiety to carbon-2, results in **17a**, which can then form pyranyl radical upon loss of the bridging CO_2 (**18a**). The second possible pathway for **22c** decomposition involves scission of the C_6−O bond to provide 1,6-oxohex-2,4-en-1-oxy radical (**20b**). After expulsion of CO_2 from **20b**, **24a** is formed, providing another intersection with a 2-peroxyoxepinone radical (**1a**) process (Figure 3), which has CO_2, C_2H_2, $O(^3P)$, and 3-oxo-1-propen-1-yl radical (**25a**) as products.

C. Comparison of Decomposition Pathways from 298 to 1250 K. To contrast all of the proposed decomposition pathways (Figures 3−5) as a function of temperature, the free energy profiles for all intermediates and transition states in each pathway at 298, 500, 750, 1000, and 1250 K have been plotted

TABLE 3: Relative Gibbs Free Energies for All Intermediates and Transition States (298−1250 K) at the B3LYP/6-311+G// B3LYP/6-31G* Level Related to 1c Decomposition**

structure[a]	E[b] (hartrees/part)	ΔG(298 K) (kcal/mol)	ΔG(500 K) (kcal/mol)	ΔG(750 K) (kcal/mol)	ΔG(1000 K) (kcal/mol)	ΔG(1250 K) (kcal/mol)	$\langle S^2 \rangle$	other (PG, ES, N_{imag})[c]
TS (1−1c)	−532.50740	17.5	24.7	33.6	42.4	51.2	1.09	C_1, −, 1
1c	−532.52526	9.0	17.0	26.7	36.2	45.6	0.75	C_1, −, 0
TS (1c−2c)	−532.46008	46.0	53.9	63.6	73.2	82.6	0.77	C_1, −, 1
2c	−532.54729	−6.9	0.1	8.5	16.6	24.5	0.78	C_1, −, 0
TS (2c−3c)	−532.54723	−7.9	−0.8	7.9	16.4	24.9	0.80	C_1, −, 1
3c[d]	−532.58274	−41.4	−41.3	−41.4	−41.5	−41.5	0	C_1, −, 0
TS (1c−4c)	−532.49135	30.2	38.9	49.8	60.7	71.5	0.79	C_1, −, 1
4c	−532.50668	20.9	29.2	39.4	49.5	59.4	0.78	C_1, −, 0
TS (4c−5c)	−532.48428	33.6	41.8	52.0	62.2	72.4	0.99	C_1, −, 1
5c	−532.56092	−12.9	−4.3	6.3	16.7	26.9	0.75	C_1, −, 0
TS (5c−6c)	−532.53662	−0.3	7.8	17.8	27.8	37.6	0.77	C_1, −, 1
6c	−532.56802	−21.1	−14.7	−7.0	0.5	7.8	0.76	C_1, −, 0
TS (6c−7c)	−532.55245	−14.0	−8.3	−1.4	5.5	12.2	0.76	C_1, −, 1
7c[e]	−532.57137	−35.5	−36.2	−37.1	−38.0	−39.0	0.76	C_1, −, 0
TS (7c−8c)[e]	−532.56289	−30.4	−30.5	−30.6	−30.5	−30.3	0.76	C_1, −, 1
8c[e]	−532.56613	−32.4	−33.0	−34.0	−34.9	−35.9	0.76	C_1, −, 0
TS (8c−9c)[e]	−532.56140	−29.5	−29.7	−29.9	−29.9	−29.8	0.76	C_1, −, 1
9c[e]	−532.57077	−35.5	−36.4	−37.7	−38.9	−40.2	0.76	C_1, −, 0
TS (9c−10c)[e]	−532.55503	−27.1	−26.9	−26.7	−26.4	−26.1	0.76	C_1, −, 1
10c[e]	−532.60727	−57.3	−58.1	−59.2	−60.2	−61.2	0.75	C_1, −, 0
TS (10c−11c)[e]	−532.57797	−42.9	−45.2	−48.0	−50.7	−53.2	0.76	C_1, −, 1
11c[f]	−532.58234	−55.1	−63.2	−27.8	−83.1	−92.8	0.75	C_1, −, 0
TS (11c−12c)[f]	−532.57238	−50.0	−58.0	−20.6	−77.1	−86.3	0.76	C_1, −, 1
12c[f]	−532.66042	−104.5	−112.9	−123.3	−133.6	−143.7	0.78	C_1, −, 0
TS (1c−13c)	−532.47794	38.8	47.8	59.0	70.2	81.3	0.81	C_1, −, 1
13c	−532.50669	21.4	30.1	40.8	51.3	61.7	0.75	C_1, −, 0
TS (13c−14c)	−532.46387	45.1	53.1	62.9	72.7	82.3	0.78	C_1, −, 1
14c	−532.45970	46.6	53.3	61.2	68.9	76.4	0.76	C_1, −, 0
TS (14c−15c)	−532.41875	68.9	74.6	81.2	87.6	93.9	0.77	C_1, −, 1
15c[g]	−532.40469	48.6	48.1	47.2	46.1	45.0	0.75	C_1, −, 0
TS (15c−14a)[g]	−532.38842	56.7	56.0	54.8	53.6	52.4	0.76	C_1, −, 1
TS (13c−16c)	−532.48962	30.5	39.1	49.7	60.2	70.7	0.77	C_1, −, 1
16c	−532.59437	−35.8	−28.5	−19.6	−10.8	−2.2	0.75	C_1, −, 0
TS (16c−17c)	−532.57602	−26.3	−18.4	−8.6	1.1	10.7	0.76	C_1, −, 1
17c	−532.61487	−47.9	−40.6	−31.8	−23.2	−14.7	0.75	C_1, −, 0
TS (17c−18c)	−532.59781	−39.5	−32.7	−24.4	−16.2	−8.0	0.76	C_1, −, 1
18c[h]	−532.61104	−59.4	−59.7	−60.2	−60.7	−61.3	0.76	C_1, −, 0
TS (18c−19c)[h]	−532.58952	−47.7	−48.2	−48.8	−49.4	−49.9	0.77	C_1, −, 1
19c[i]	−532.58369	−54.7	−61.5	−70.1	−78.5	−86.8	0	C_1, −, 0
TS (1c−15a)	−532.49778	26.5	35.5	46.7	57.9	69.0	0.80	C_1, −, 1
TS (15a−20c)	−532.50011	23.9	32.5	43.1	53.7	64.3	0.76	C_1, −, 1
20c[e]	−532.65587	−88.3	−89.1	−90.1	−91.1	−92.1	0.79	C_2, ^{2}A, 0
TS (20c−21c)[e]	−532.62323	−67.3	−67.2	−66.9	−66.4	−65.8	0.76	C_1, −, 1
21c[e]	−532.65583	−86.9	−87.0	−87.1	−87.2	−87.3	0.77	C_1, −, 0
TS (21c−10a)[e]	−532.62343	−68.2	−68.5	−68.7	−68.8	−68.8	0.77	C_1, −, 1
TS (1c−22c)	*k*							
22c[j]	−532.40773	52.1	53.2	54.3	55.3	56.2	0.76	C_1, −, 0
TS (22c−17a)[j]	−532.39825	58.7	60.9	63.7	66.4	69.2	0.78	C_1, −, 1
TS (22c−20b)[j]	−532.36788	75.3	76.4	77.6	78.7	79.8	0.78	C_1, −, 1

[a] See Figure 5 for structures. [b] Bottom-of-the-well energy. [c] Point group (PG), electronic state (ES), number of imaginary vibrational frequencies (N_{imag}). [d] E and $\Delta G(T)$ values include E and $G(T)$ of OH. [e] E and $\Delta G(T)$ values include E and $G(T)$ of CO_2. [f] E and $\Delta G(T)$ values include E and $G(T)$ of CO and CO_2. [g] E and $\Delta G(T)$ values include E and $G(T)$ of C_2H_2. [h] E and $\Delta G(T)$ values include E and $G(T)$ of CO. [i] E and $\Delta G(T)$ values include E and $G(T)$ of CO and OH. [j] E and $\Delta G(T)$ values include E and $G(T)$ of $O(^3P)$. [k] A reliable transition state was not found for this process.

and are shown in Figures 6−8 for the decomposition of **1a**, **1b**, and **1c**, respectively. Additionally, the bottom-of-the-well electronic energies and Gibbs free energies at 298, 500, 750, 1000, and 1250 K for all intermediates and transition states, relative to **1**, as well as the $\langle S^2 \rangle$ value, point group, electronic state, and number of imaginary vibrational frequencies are listed in Tables 1−3 for decomposition of **1a**, **1b**, and **1c**, respectively.

The free energy of activation barriers for the addition of molecular oxygen to 2-oxepinoxy radical (**1**) increase from ∼17 kcal/mol at 298 K to ∼50 kcal/mol at 1250 K. The relative ordering of the free energies of activation remains unchanged through this temperature regime with **TS (1−1b)** being the lowest energy barrier throughout the temperature range (Table 1). The barrier for formation of either of the peroxyoxepinone radicals is not the highest point on the free energy surface for any of the proposed decomposition pathways at any of the temperatures considered. Despite the large barrier for O_2 addition and small endoergicity of formation of each of the peroxyoxepinone radicals, their free energies are still well below that of phenyl radical and 2 $O_2(^3\Sigma_g)$ molecules at temperatures <1250 K due to the large exoergic formation of 2-oxepinoxy radical (**1**). The free energy of phenyl radical and two molecular oxygens, relative to **1** and O_2, are +80.4, +73.3, +64.7, +56.3, and +48.0 kcal/mol at 298, 500, 750, 1000, and 1250 K, respectively.

Figure 6 shows the free energy profiles for the decomposition pathways of **1a.** At 298 K, the unimolecular decomposition of **1a** through **15a** is the lowest energy process. The complete free

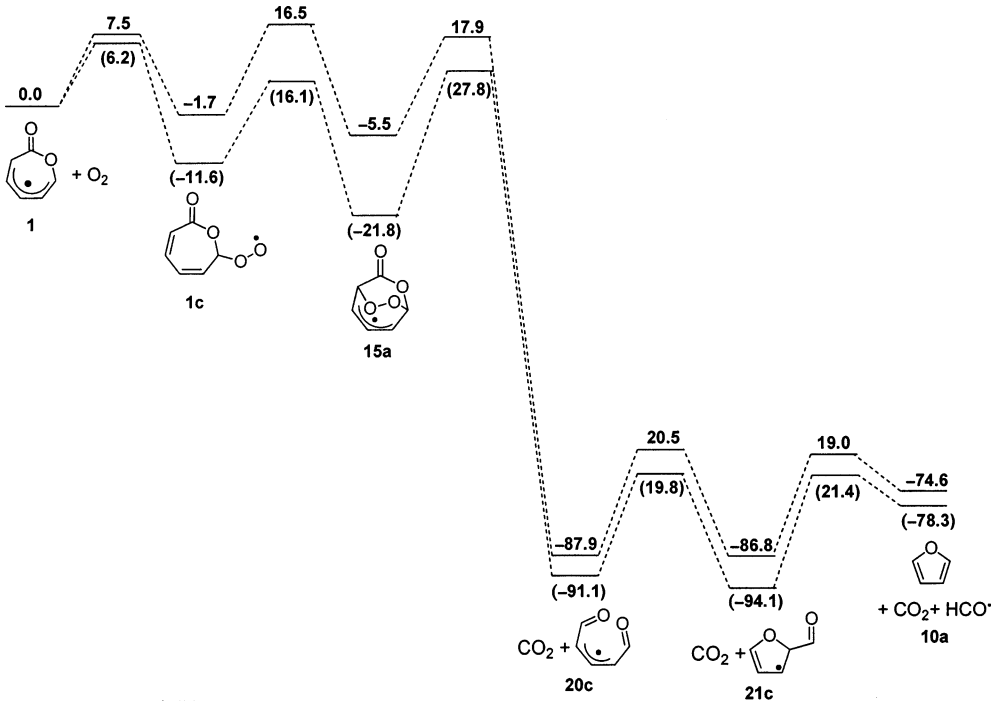

Figure 9. Potential energy surfaces (ΔH, kcal/mol at 0 K) at the B3LYP/6-311+G**//B3LYP/6-31G* and CBS-QB3 (parentheses) levels for the lowest energy pathway for the oxygen initiated decomposition of 2-oxepinoxy radical (**1**). The energies for each intermediate are relative to **1** and each barrier is relative to the reactant for that specific step.

energy profile for decomposition of **15a** is shown in Figure 8, where **15a** also emanates from **1c**. Regardless, the free energy barrier for **1a** or **1b** to form **15a** is the highest point on the energy profile, irrespective of whether the reactant is **1a** or **1b**. Thermodynamically, furan, CO_2, and formyl radical (**10a**) as products represent the most exoergic pathway (ΔG(298 K) = −84.9 kcal/mol) formed from the dioxetanyl intermediate (**4a**) via **1b** → **4a** → **5a** → **8a** → **9a** → **10a**. Pathways resulting from the peroxy O−O bond scission intermediate lie near the top of the 298 K free energy profile for **1a** decomposition. Furthermore, the only exoergic intermediate or product at 298 K is **18a** starting from the decomposition of **16a**. The high-energy profile for decomposition of **16a** can be attributed to the unfavorability of generating free oxygen atom at low temperatures. Next to the formation of **15a**, the lowest profile is through **4a** followed by **26a**. With increasing temperature through to 1250 K, the free energy profiles for the rearrangement pathways increase steadily, with the ordering between pathways remaining generally consistent. The increasing height of the **1a** free energy profiles is due to a small negative value for the entropy of the addition step of molecular oxygen to 2-oxepinoxy radical (**1**). In contrast, the free energy profiles for **1a** decomposition through **16a** remain approximately constant through the first few steps, after which they become exoergic, due to an increased influence of entropy, resulting from breaking the peroxy O−O bond to generate the oxygen atom. At 1250 K, the decomposition pathways through the O−O scission intermediate **16a** have lower overall free energy profiles than those through rearrangement intermediates. However, the profile through **15a** remains the lowest of the rearrangement profiles. The formation of **10a** (furan, CO_2, and formyl radical) is the most stable overall product of **1a** decomposition throughout the 298−1250 K temperature range. Between 500 and 750 K, the free energies for rearrangement and decomposition through the chosen intermediates start to become uncompetitive with respect to the energy of phenyl radical and 2 oxygen molecules as well as the "Fadden" pathways for unimolecular decomposition of **1**.[31]

The free energy profiles for the decomposition pathways of **1b** and **1c** (Figures 7 and 8, respectively) are qualitatively similar to those for **1a**. At 298 K, the lowest overall profile for decomposition of **1b** is through **11a**, resulting in formation of **7a** (Figure 7). The highest free energy profile at 298 K is for decomposition through peroxy O−O bond scission (**17b**). Thermodynamically, **16b** products, formed via the dioxetanyl intermediate **8b,** provide the most exoergic pathway for the decomposition of **1b** at all temperatures. Though the profile trends for **1b** are consistent with those of **1a** as the temperature is increased, pathways through **17b** become lower in energy and sufficiently competitive with the other pathways at 1250 K. The lowest overall free energy pathway at 298 K is for the profile **1c** → **15a** → **20c** → **21c** → **10a** (Figure 8) and remains the lowest profile up to 1250 K, wherein the pathway of **1c** → **22c** → **17a** → **18a** is slightly lower ($\Delta G^{\ddagger}$(1250 K) = 68.6 kcal/mol vs 69 kcal/mol). The overall most exoergic pathway at all temperatures corresponds to formation of **12c** followed by **10a**.

D. Comparison of DFT Energetics. Due to a lack of experimental data for the energetics of the intermediates proposed in the preceding pathways, CBS-QB3 optimization and energy calculations were performed on the three 2-oxepinoxy + O_2 addition steps as well as the lowest energy pathway, **1c** → **10a**, via the 1,4-peroxy intermediate **15a**. Table 4 lists the ΔH(298 K) and ΔG(298 K) values for the intermediates and the transition states for the interconversion of **1** → **1a**, **1** → **1b**, **1** → **1c**, and **1c** → **10a** at the B3LYP/6-311+G**//B3LYP/6-31G* and CBS-QB3 levels. Figure 9 illustrates the relative ΔH(0 K) values for the **1c** → **10a** pathway. The $\Delta G^{\ddagger}$(298 K) values for addition of molecular oxygen at the CBS-QB3 level agree well with those obtained using our DFT method, differing at most by 2 kcal/mol for addition of O_2 to carbon-4 of **1**. The three peroxyoxepinone (**1a**, **1b**, and **1c**) free energies at 298 K,

TABLE 4: Relative Energies (kcal/mol) of Selected Intermediates at the B3LYP/6-311+G//B3LYP/6-31G* and CBS-QB3 Levels**

	B3LYP[a]		CBS-QB3	
molecule	ΔH(298 K)	ΔG(298 K)	ΔH(298 K)	ΔG(298 K)
1	0.0	0.0	0.0	0.0
TS (1−1a)	7.5	17.7	5.8	16.9
TS (1−1b)	7.2	17.0	4.6	15.0
TS (1−1c)	7.5	17.6	5.6	16.2
1a	−0.4	10.4	−11.1	0.7
1b	3.4	13.2	−5.3	5.1
1c	−1.7	9.0	−12.5	−0.8
TS (1c−15a)	14.8	26.5	3.1	16.2
15a	−5.5	6.4	−23.3	−9.9
TS (15a−20c)	12.4	23.9	4.7	17.6
20c	−87.9	−88.7	−90.5	−91.9
TS (20c−21c)	−67.4	−67.3	−71.4	−71.2
21c	−86.8	−86.9	−94.1	−94.1
TS (21c−10a)	−67.8	−68.2	−72.7	−73.0
10a	−74.6	−85.3	−77.5	−88.8

[a] Energies correspond to the B3LYP/6-311+G**//B3LYP/6-31G* level.

on the other hand, appear to be significantly underestimated by the B3LYP method. The difference in ΔG(298 K) between the two methods, for the peroxyoxepinone intermediates, range from 8.1 to 9.8 kcal/mol, with the CBS-QB3 method giving more exoergic values. The difference in ΔG(298 K) increases upon formation of **15a** to 16.3 kcal/mol, approximately double that for the O_2 addition products (**1a**, **1b** and **1c**). This trend is conserved in the ΔH(0 K) and ΔH(298 K) energy values, and this discrepancy is obviously not due to thermal and entropic corrections alone. The origin of this discrepancy is not clear at this time. These calculations have been performed with single-reference wave functions, and perhaps some multiconfigurational character is important for the peroxy species derived from unsaturated radicals.

The agreement between the 298 K free energy of activation barrier heights for the B3LYP and CBS methods is consistent, throughout the **1c → 15a → 20c → 21c → 10a** pathway, with values differing on average by 2.4 kcal/mol. There is a large discrepancy, however, between the barrier heights for **TS (15a−20c)** of ∼10 kcal/mol. Following decomposition of the peroxy moiety, the ΔG(298 K) values fall into closer agreement. Despite the discrepancy in reaction free energies, the qualitative nature of the B3LYP decomposition paths are in very good agreement with the CBS-QB3 method.

IV. Conclusions

Numerous possible pathways for the decomposition of 2-, 4-, and 6-peroxyoxepinone radicals (**1a**, **1b**, and **1c**), following addition of O_2 to 2-oxepinoxy radical (**1**) have been examined in the 298−1250 K temperature range. Pathways initiated via rearrangement to a dioxetane (1,2-peroxy), 1,3-peroxy, and 1,4-peroxy or by intramolecular hydrogen-atom abstraction are competitive at temperatures <500 K with the pathways proposed by Fadden[31] for the unimolecular decomposition of 2-oxepinoxy radical (**1**) in the high-pressure limit. For the decomposition of the peroxyoxepinone radicals, the mechanistic sequence of **1c → 15a → 20c → 21c → 10a** appears to be the most viable pathway. Due to the large exoergicity associated with forming 2-oxepinoxy radical, these rearrangement pathways all lie below the level of free energy to regenerate phenyl radical and two O_2 molecules. However, as the temperature becomes greater than 500 K, the overall barriers for the proposed pathways make them less competitive, as a result of unfavorable entropy associated with the addition step of O_2 to 2-oxepinoxy radical as compared to previously calculated pathways for unimolecular decomposition mechanisms.[31]

The present paper reflects an attempt to estimate the competition of oxidative interference on the unimolecular decomposition products of phenylperoxy radical that generates 2-oxepinoxy radical in a very exothermic reaction. Due to the complex physical and chemical nature of combustion environments as well as the high exothermicity for the initial generation of 2-oxepinoxy radical, a more thorough treatment of the branching pathways via a multiwell master-equation analysis may also be warranted.

Acknowledgment. We gratefully acknowledge The Ohio State University Environmental Molecular Science Institute (EMSI) funded by NSF, the Ohio Supercomputer Center, the Department of Energy, a GAANN and Amoco Fellowship to J.K.M. We also thank Paul R. Rablen (Swarthmore College) for providing his Thermo94 program.

Supporting Information Available: Energies, enthalpies, free energies as a function of temperature, and moments of inertia for all intermediates and transition states. Cartesian coordinates and harmonic vibrational frequencies for all intermediates and transition states. This material is available free of charge via the Internet at http://pubs.acs.org.

References and Notes

(1) Santos, C. Y. M.; Almeida Azevedo, D.; Aquino Neto, F. R. *Atmos. Environ.* **2004**, *38*, 1247−1257.
(2) Burri, J.; Crockett, R.; Hany, R.; Rentsch, D. *Fuel* **2004**, *83*, 187−193.
(3) Yamada, E.; Hosokawa, Y.; Furuya, Y.; Matsushita, K.; Fuse, Y. *Anal. Sci.* **2004**, *20*, 107−112.
(4) Schuetzle, D.; Siegl, W. O.; Jensen, T. E.; Dearth, M. A.; Kaiser, E. W.; Gorse, R.; Kreucher, W.; Kulik, E. *Environ. Health Persp.* **1994**, *102* (S4), 3−12.
(5) Richter, H.; Howard, J. B. *Prog. Energy Combust. Sci.* **2000**, *26*, 565−608.
(6) Marsh, N. D.; Ledesma, E. B.; Sandrowitz, A. K.; Wornat, M. J. *Energy Fuels* **2004**, *18*, 209−217.
(7) Venkat, C.; Brezinsky, K.; Glassman, I. *Symp. (Int.) Combust., 19th* **1982**, 143−152.
(8) Rotzoll, G. *Int. J. Chem. Kinet.* **1985**, *17*, 637−653.
(9) Frank, P.; Herzler, J.; Just T.; Wahl, C. *Symp. (Int.) Combust., 25th* **1994**, 833−840.
(10) Bermudez, G.; Pfefferle, L. *Combust. Flame* **1995**, *100*, 41−51.
(11) Chai, Y.; Pfefferle, L. D. *Fuel* **1998**, *77*, 313−320.
(12) Yu, T.; Lin, M. C. *J. Am. Chem. Soc.* **1994**, *116*, 9571−9576.
(13) Norrish, R. G. W.; Taylor, G. W. *Proc. R. Soc.* **1965**, *A234*, 160−177.
(14) Carpenter, B. K. *J. Am. Chem. Soc.* **1993**, *113*, 9806−9807.
(15) Barckholtz, C.; Fadden, M. J.; Hadad, C. M. *J. Phys. Chem. A* **1999**, *103*, 8108−8117.
(16) Fadden, M. J.; Barckholtz, C.; Hadad, C. M. *J. Phys. Chem. A* **2000**, *104*, 3004−3011.
(17) Ruifeng, L.; Morokuma, K.; Mebel, A. M.; Lin, M. C. *J. Phys. Chem.* **1996**, *100*, 9314−9322.
(18) Mebel, A. M.; Lin, M. C. *J. Am. Chem. Soc.* **1994**, *116*, 9577−9584.
(19) Cioslowski, J.; Liu, G.; Martinov, M.; Piskorz, P.; Moncrieff, D. *J. Am. Chem. Soc.* **1996**, *118*, 5261−5264.
(20) Barckholtz, C.; Barckholtz, T. A.; Hadad, C. M. *J. Am. Chem. Soc.* **1999**, *121*, 491−500.
(21) Frisch, M. J.; Trucks, G. W.; Schlegel, H. B.; Scuseria, G. E.; Robb, M. A.; Cheeseman, J. R.; Zakrzewski, V. G.; Montgomery, J. A., Jr.; Stratmann, R. E.; Burant, J. C.; Dapprich, S.; Millam, J. M.; Daniels, A. D.; Kudin, K. N.; Strain, M. C.; Farkas, O.; Tomasi, J.; Barone, V.; Cossi, M.; Cammi, R.; Mennucci, B.; Pomelli, C.; Adamo, C.; Clifford, S.; Ochterski, J.; Petersson, G. A.; Ayala, P. Y.; Cui, Q.; Morokuma, K.; Malick, D. K.; Rabuck, A. D.; Raghavachari, K.; Foresman, J. B.; Cioslowski, J.; Ortiz, J. V.; Stefanov, B. B.; Liu, G.; Liashenko, A.; Piskorz, P.; Komaromi, I.; Gomperts, R.; Martin, R. L.; Fox, D. J.; Keith, T.; Al-Laham, M. A.; Peng, C. Y.; Nanayakkara, A.; Gonzalez, C.; Challacombe, M.; Gill, P. M. W.; Johnson, B.; Chen, W.; Wong, M. W.; Andres, J. L.; Gonzalez, C.;

Head-Gordon, M.; Replogle, E. S.; Pople, J. A. *Gaussian 98*, revision A.7; Gaussian, Inc.: Pittsburgh, PA, 1998.

(22) Becke, A. D. *J. Chem. Phys.* **1993,** 98, 5648.

(23) Lee, C.; Yang, W.; Par, R. G. *Phys. Rev. B* **1998**, 37, 785−789.

(24) Hehre, W. J.; Radom, L.; Schleyer, P. v. R.; Pople, J. A. *Ab Initio Molecular Orbital Theory*; John Wiley & Sons: New York, 1986.

(25) Bauschlichter, C. W., Jr.; Langhoff, S. R. *Mol. Phys.* **1999**, 96, 471.

(26) (a) Gonzalez, C.; Schlegel, H. B. *J. Chem. Phys.* **1989**, 90, 2154. (b) Gonzalez, C.; Schlegel, H. B. *J. Phys. Chem.* **1990**, *94*, 5523.

(27) Rablen, P. R. *Thermo94*; Yale University: New Haven, CT, 1994.

(28) Reference 29 recommends that B3LYP/6-31G(d) vibrational frequencies used for the determination of $\Delta H_{vib}(T)$ and $\Delta S_{vib}(T)$ be scaled by 0.9989 and 1.0015, respectively. However, considering how close those values are to 1, we have chosen to leave the frequencies unscaled for simplicity.

(29) Scott, A. P.; Radom, L. *J. Phys. Chem.* **1996**, *100*, 16502−16513.

(30) Montgomery, J. A., Jr.; Frisch, M. J.; Ochterski, J. W.; Petersson, G. A. *J. Chem. Phys.* **1999**, *110*, 2822−2827.

(31) Fadden, M. J.; Hadad, C. M. *J. Phys. Chem. A* **2000**, 104, 8121−8130.